PG
Petroleum Geoscience

Research article

Published Online First

https://doi.org/10.1144/petgeo2019-126

Fault seal modelling – the influence of fluid properties on fault sealing capacity in hydrocarbon and CO_2 systems

Rūta Karolytė[1]*, Gareth Johnson[2], Graham Yielding[3] and Stuart M.V. Gilfillan[2]

[1] Department of Earth Sciences, University of Oxford, 3 South Parks Road, Oxford OX1 3AN, UK
[2] School of GeoSciences, University of Edinburgh, James Hutton Road, Edinburgh EH9 3FE, UK
[3] Badley Geoscience Ltd, North Beck House, North Beck Lane, Spilsby PE23 5NB, UK

RK, 0000-0002-8114-4297; GJ, 0000-0002-3151-5045; SMVG, 0000-0003-1929-2843

* Correspondence: ruta.karolyte@earth.ox.ac.uk

Present addresses: GJ, Department of Civil and Environmental Engineering, University of Strathclyde, James Weir Building, 75 Montrose Street, Glasgow G1 1XJ, UK

Abstract: Fault seal analysis is a key part of understanding the hydrocarbon trapping mechanisms in the petroleum industry. Fault seal research has also been expanded to CO_2–brine systems for the application to carbon capture and storage (CCS). The wetting properties of rock-forming minerals in the presence of hydrocarbons or CO_2 are a source of uncertainty in the calculations of capillary threshold pressure, which defines the fault sealing capacity. Here, we explore this uncertainty in a comparison study between two fault-sealed fields located in the Otway Basin, SE Australia. The Katnook Field in the Penola Trough is a methane field, while Boggy Creek in Port Campbell contains a high-CO_2–methane mixture. Two industry standard fault seal modelling methods, one based on laboratory measurements of fault samples and the other based on a calibration of a global dataset of known sealing faults, are used to discuss their relative strengths and applicability to the CO_2 storage context. We identify a range of interfacial tensions and contact angle values in the hydrocarbon–water system under the conditions assumed by the second method. Based on this, the uncertainty related to the spread in fluid properties was determined to be 24% of the calculated threshold capillary pressure value. We propose a methodology of threshold capillary pressure conversion from hydrocarbons–brine to the CO_2–brine system, using an input of appropriate interfacial tension and contact angle under reservoir conditions. The method can be used for any fluid system where fluid properties are defined by these two parameters.

Supplementary material: (1) Fault seal modelling methods and calculations, and (2) hydrocarbon and CO_2 interfacial tensions and contact angle values collected in the literature are available at https://doi.org/10.6084/m9.figshare.c.4877049

This article is part of the Energy Geoscience Series available at https://www.lyellcollection.org/cc/energy-geoscience-series

Received 1 October 2019; **revised** 17 February 2020; **accepted** 1 March 2020

Faults can be either pathways for, or barriers to, fluid migration in the subsurface and to the surface. Fault seal analytical techniques have been developed to improve the prediction of hydrocarbon traps suitable for exploration. More recently, fault seal research has expanded to applications to carbon capture and storage (CCS), where faults can act to: decrease the maximum storage capacity of the reservoir; become unwanted barriers to fluid migration along the planned injection pathway, causing pressure increase and limiting the maximum rate of injection; or provide a conduit for leakage of CO_2.

Two distinct methodologies of predictive modelling of the threshold capillary pressure, which is a proxy for fault sealing capacity to hydrocarbons, have been developed in the last two decades: one based on a calibration of a global dataset of known sealing faults (Bretan *et al.* 2003; Yielding *et al.* 2010) and another based on laboratory measurements of fault samples (Sperrevik *et al.* 2002). Both of these techniques have been widely applied to hydrocarbon systems. Fault capacity to seal for CO_2 has been explored in theoretical studies (Naylor *et al.* 2010; Iglauer 2018; Miocic *et al.* 2019), yet there have been few attempts to test the methodology with real geological examples (Bretan *et al.* 2011; Yielding *et al.* 2011; Bretan 2016).

In terms of practically applying model results to either exploration of hydrocarbons or CO_2 sequestration, the subject of interest is not the exact threshold capillary pressure of a certain fault but, rather, the implications of that value to the desired industrial activity. In exploration, this is applied to estimate maximum column height and determine the economic viability of production. It is therefore important to estimate how the uncertainty associated with the predictive method impacts the prospect. In the context of CO_2 storage, threshold capillary pressure is used to define the reservoir storage capacity. In this case, the aim is not to overpressure the fault and thus cause leakage. The practical use of fault seal modelling therefore requires a good understanding of the uncertainty associated with the two different approaches.

The interfacial tension (IFT) and the contact angle (CA) are the main fluid-specific properties controlling the capillary seal and the key parameters used in both hydrocarbon and CO_2 studies. The wetting properties of various rock-forming minerals are different for CO_2 and hydrocarbons, which has caused a concern that the seal rocks proven to retain hydrocarbon columns might be less sealing to CO_2 (Chiquet *et al.* 2007*b*; Daniel and Kaldi 2009; Tenthorey *et al.* 2014; Guariguata-Rojas and Underhill 2017). A recent study by Miocic *et al.* (2019) explored the interplay between uncertainties in CA, IFT and fault rock composition in the CO_2–brine system. The results highlighted that higher phyllosilicate content in the fault rock reduces the threshold capillary pressure in the CO_2–brine system due to the wettability of the clay minerals in the presence of CO_2, especially at depths of >1 km.

Our understanding of CA and IFT primarily relies on empirical measurements, meaning that significant uncertainty exists in both hydrocarbons–brine and CO_2–brine systems. While the above concerns are valid for the CO_2 storage, the existing uncertainties associated with CA and IFT also exist in the hydrocarbons. This is

because of the wide range of chemical compositions of crude oil and the difficulty of sampling undegassed reservoir fluids.

In this contribution, we investigate the uncertainty associated with the fluid properties (CA and IFT), as well as the geological assumptions required for the model (depth at the time of faulting and maximum burial depth) in two field examples: a methane gas field in South Australia (Katnook) and a high CO_2–methane mixture in Port Campbell, Victoria (Boggy Creek). In both cases, a gas column is supported by the fault rock and the column height is known. The fields are located in the Otway Basin, which is very well characterized in respect of hydrocarbon exploration, as well as CO_2 storage. These case studies therefore provide a realistic example of the level of uncertainties that can be expected in future potential CO_2 storage sites.

This approach allows us to verify if the model predictions are valid, and systematically compare the uncertainties in the CO_2 and methane system. Fault seal analysis is performed using the Sperrevik *et al.* (2002) and Yielding *et al.* (2010) fault seal modelling methods. The objective is to discuss the differences in the modelling approaches, their associated uncertainties and suitability for the CO_2–brine system. The former method inherently allows the conversion from a mercury–air system to CO_2–brine, while the latter method is calibrated to a hydrocarbon system. We summarize the current understanding of the IFT and CA ranges in hydrocarbons that the Yielding *et al.* (2010) method is based on to define the expected IFT and CA distribution and their mean values. Based on this, we propose a new calibration of the Yielding *et al.* (2010) algorithm to the CO_2–brine system.

Fault rock seal dependencies

Fault rock seals occur when movement along a fault plane creates a low-permeability fault rock and depend on the fault rock composition, as well as the properties of the fluids in the system. In siliciclastic sand–shale sequences, the sealing fault rocks are characterized by continuous clay-rich smears (Lindsay *et al.* 1993). Their thickness is favoured by a greater thickness of shale beds in host rocks, weight of the overburden and burial depth (Lehner and Pilaar 1997). Quartz cementation at temperatures above 90°C or at depths of more than 3 km further decreases fault rock porosity and increases the sealing potential (Rimstidt and Barnes 1980; Fisher and Knipe 1998). The resulting fault rock may act as baffle to fluid migration through a process of capillary sealing, which is created by the opposing forces between the two phases at their interface – the wetting phase (water or brine) and the non-wetting phase (hydrocarbons or CO_2, in this context) (Watts 1987; Yielding *et al.* 1997; Fisher and Knipe 1998). Capillary seals fail when the fluid buoyancy pressure exceeds the threshold capillary pressure. Capillary threshold pressure (P_c) is therefore a key fault rock attribute used in the hydrocarbon exploration industry to determine the sealing potential of the fault and to calculate maximum column heights (h_{max}), using the relationship between the height of the fluid column and the buoyancy pressure it exerts on the sealing rocks (Schowalter 1974):

$$P_c = \frac{2\text{IFT} \times \cos\theta}{r} \quad (1)$$

$$h_{max} = \frac{P_c}{(\rho_h - \rho_w)g} \quad (2)$$

where IFT is the interfacial tension between the fluids, θ is the CA, r is the effective pore throat radius, ρ is density, g is acceleration due to gravity, and subscripts h and w denote hydrocarbons and water, respectively.

The IFT and CA (or wettability) are the key properties controlling capillary seal, and depend on many factors including pressure, temperature, fluid type, fluid density and rock mineralogy (e.g. Schowalter 1974; Radke *et al.* 1992; Øren and Bakke 2003; Nordgard Bolas *et al.* 2005; Iglauer *et al.* 2015). The influence of these factors is a key concern in describing fault zone behaviour. The advantage, however, is that the characteristics of fluids and their affinity to reservoir rock can be approximated by these two input parameters, and therefore applied in the same manner to systems involving hydrocarbons, CO_2 or any other fluid type of interest.

The buoyancy pressure exerted on the fault rock by the column of fluid is greater with increasing density contrast between the wetting and the non-wetting phases. Under typical reservoir conditions, the density of methane ranges between 100 and 300 kg m^{-3}, CO_2 is *c.* 400–600 kg m^{-3}, and oil density varies between 700 and 1000 kg m^{-3} (Danesh 1998). Brine density depends on salinity and has a value of 1000–1150 kg m^{-3}. It is therefore apparent that a fault rock with a certain capillary threshold pressure would retain a smaller column of methane than of CO_2 or oil, if the other parameters were the same. However, the differences in interfacial tension and CA between CO_2 and hydrocarbons also impact the threshold capillary pressure of the fault rock in a CO_2–brine system (Chiquet *et al.* 2007*b*). The interplay between IFT, CA and fluid density is therefore key to consider in applying fault seal modelling techniques to CO_2 sequestration.

The effective pore throat radius of a fault zone is impossible to determine directly, and by standard practice is approximated using a predictive algorithm based on the clay content of the faulted rocks. Examples include clay smear potential (CSP) (Bouvier *et al.* 1989; Fulljames *et al.* 1997), shale smear factor (SSF) (Lindsay *et al.* 1993) and shale gouge ratio (SGR) (Yielding *et al.* 1997). We use SGR in this study due to its direct calibration to threshold capillary pressures and, in turn, gas column heights.

Two different approaches have been developed to link SGR to capillary threshold pressure. One approach is based on laboratory experiments of mercury–air injection tests in microfault samples and subsequent correlation of measured capillary pressures to sample clay content (Sperrevik *et al.* 2002), based on earlier studies by Knipe (1997) and Gibson (1998). The second approach uses data from known hydrocarbon traps sealed by faults to empirically correlate the maximum observed buoyancy pressures (assumed equivalent to threshold pressure) to SGR values (Yielding 2002; Bretan *et al.* 2003; Yielding *et al.* 2010). The two approaches have been termed 'deterministic' and 'empirical', respectively (Yielding *et al.* 2010), and will be referred to as such in the forthcoming text. The two methods are often used in conjunction and have been shown to produce similar results in certain, but not all, SGR/burial depth configurations (Yielding *et al.* 2010). To date, the application of these methods to the CO_2–brine systems has been limited (Bretan *et al.* 2011).

The deterministic approach is based on laboratory measurements of fault rock permeability from a variety of fault structures within reservoir core samples, and requires a conversion from the mercury–air system to hydrocarbon–water or CO_2–brine system by using appropriate values for IFT and CA between the fluid and the wetting phase (Sperrevik *et al.* 2002). In contrast, the empirical approach (Yielding 2002; Bretan *et al.* 2003) is based on a calibration of SGR values and across-fault buoyancy pressure differences of known sealing faults. Importantly, the calibration includes only hydrocarbons at depths greater than 1.5 km. This means that, theoretically, the method can only be applied to fluid systems which fall within the same range of IFT and CA parameters as the hydrocarbon field used in the calibration. Further constraining this range is discussed below, before we propose a methodology to convert fault seal modelling results from a hydrocarbons–brine to a CO_2–brine system.

Geological background

In this study, we describe two gas fields in the Otway Basin, Victoria, Australia: the Katnook Field in the Penola Trough and the

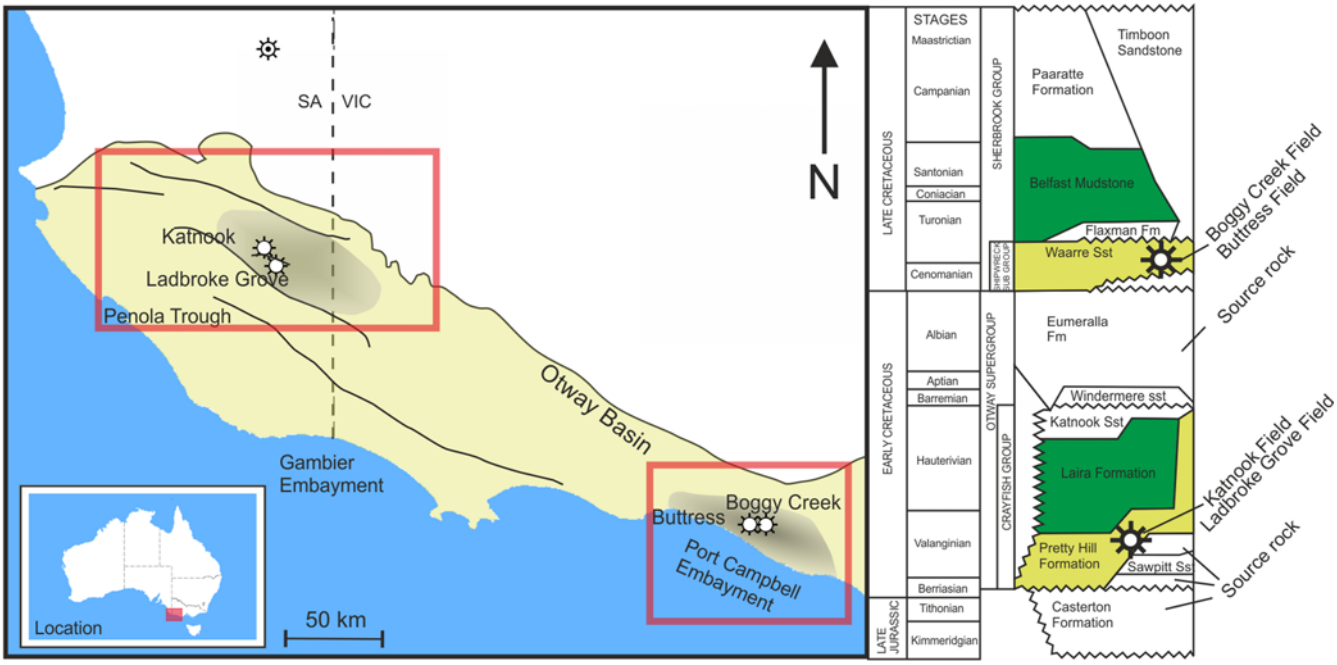

Fig. 1. Location map of the Penola Trough (Katnook and Ladbroke Grove fields) and Port Campbell (Buttress and Boggy Creek fields). Both localities are within the Otway Basin. The inset on the right shows the location of both reservoirs within the stratigraphic column (adapted from Lyon *et al.* 2004).

Boggy Creek Field in the Port Campbell embayment. In the following subsections, we outline the geology of the fields in terms of stratigraphy, trap geometries and gas charge.

Basin stratigraphy

The present-day geometry of the Otway Basin was developed during the Cretaceous–Miocene rifting with a period of inversion in the mid-Cretaceous, when the rift axis moved south (Teasdale *et al.* 2003). A series of graben and half-graben structures consist of compartmentalized fault-bound reservoirs, with numerous hydrocarbon and CO_2 accumulations (Fig. 1). Two case studies discussed here present examples of gas column retention by a fault rock in a situation of reservoir–reservoir juxtaposition: Katnook in the Penola Trough is a methane field, while the Boggy Creek field in Port Campbell contains a high-CO_2–methane mixture.

The two fields are within different reservoir formations at different stratigraphic intervals (Fig. 1). The Katnook Field is stratigraphically lower, located in Pretty Hill Formation of 2–4.5 km thickness, within the Pretty Hill Sandstone. The main target reservoir is the Pretty Hill Sandstone member at the top of the sequence (Lyon *et al.* 2005*a*, *b*). The formation consists of massive, slumped and cross-bedded sand packages, classified as lith-arenites to feldspathic lith-arenites, deposited in a continental fluvio-lacustrine environment (Little and Phillips 1995). The Laira Formation forms a regional seal, comprising siltstones and shales interbedded with sandstones. The Katnook sandstone at the top of the Crayfish Group (consisting of both the reservoir and the seal lithologies) is also gas bearing but is not a subject to this discussion. Katnook-1 and Katnook-2 are production wells targeting Katnook sandstone within the Crayfish Group, while Katnook-3 produces from the deeper Pretty Hill Formation. Shale units within the lower parts of the Pretty Hill Formation and the underlying Casterton Formation are the oil and gas source rocks in the Penola Trough and the SW part of the basin (Boreham *et al.* 2004).

The Boggy Creek CO_2 field is stratigraphically higher, within the Waarre Sandstone, comprising deltaic and shallow-marine interbedded siltstones and shales, segregated into four units defined by depositional environments. Unit C, the main reservoir interval, is poorly sorted, medium- to coarse-grained quartz arenite (Watson *et al.* 2004). The underlying Eumeralla Formation consists of interbedded lithic sandstones, siltstones, coals and claystones (Cockshell *et al.* 1995). The deeper coal-rich units of Eumeralla Formation are the source rocks in the SE part of the basin. The Belfast Mudstone overlies the reservoir and forms a regional seal (Boreham *et al.* 2004).

The Waarre Sandstone is *c*. 90 m thick and the main producing interval within it (Unit C) is 25–40 m thick (Dance 2013). The underlying Eumeralla Formation is up to 3 km thick (Cockshell *et al.* 1995). Significant oil shows have been observed within the Eumeralla Formation in other parts of the basin (Lisk 2004), and therefore good connectivity between the Waare and Eumeralla units is expected despite the silt and clay interbeds.

Trap geometry

The Katnook Field is bound by the Katnook Fault to the north and Ladbroke Grove Fault to the south (Fig. 2a). The northern side of the field is juxtaposition-sealed against Crayfish Group shales, while the southern side reaches the Ladbroke Grove Fault where the reservoir is self-juxtaposed (Fig. 2c). The fault rock supports a column of 31 m on the southern edge of the gas field; the total gas column height is 101 m. The Boggy Creek Field is bound by the Boggy Creek Fault to the south and the Buttress Fault to the north (Fig. 2b). Similarly to the Katnook Field, the main seal to the reservoir is provided by juxtaposition seal to the south (total gas column 128 m) but fault rock seal exists to the north, supporting a gas column of 51 m (Fig. 2d).

The sequence of gas charge events

The two main phases of hydrocarbon generation in the Otway Basin are estimated at mid-Cretaceous (Boult *et al.* 2004) and mid-Paleogene (Duddy 1997), based on thermal maturation modelling and the relationship between gas–water contact (GWC) positions above spill points and known gas diffusion rates (Lyon *et al.* 2005*a*). Early oil/wet gas charge was flushed or diluted by later dry gas charge (Boreham *et al.* 2004). Methane charge was followed by

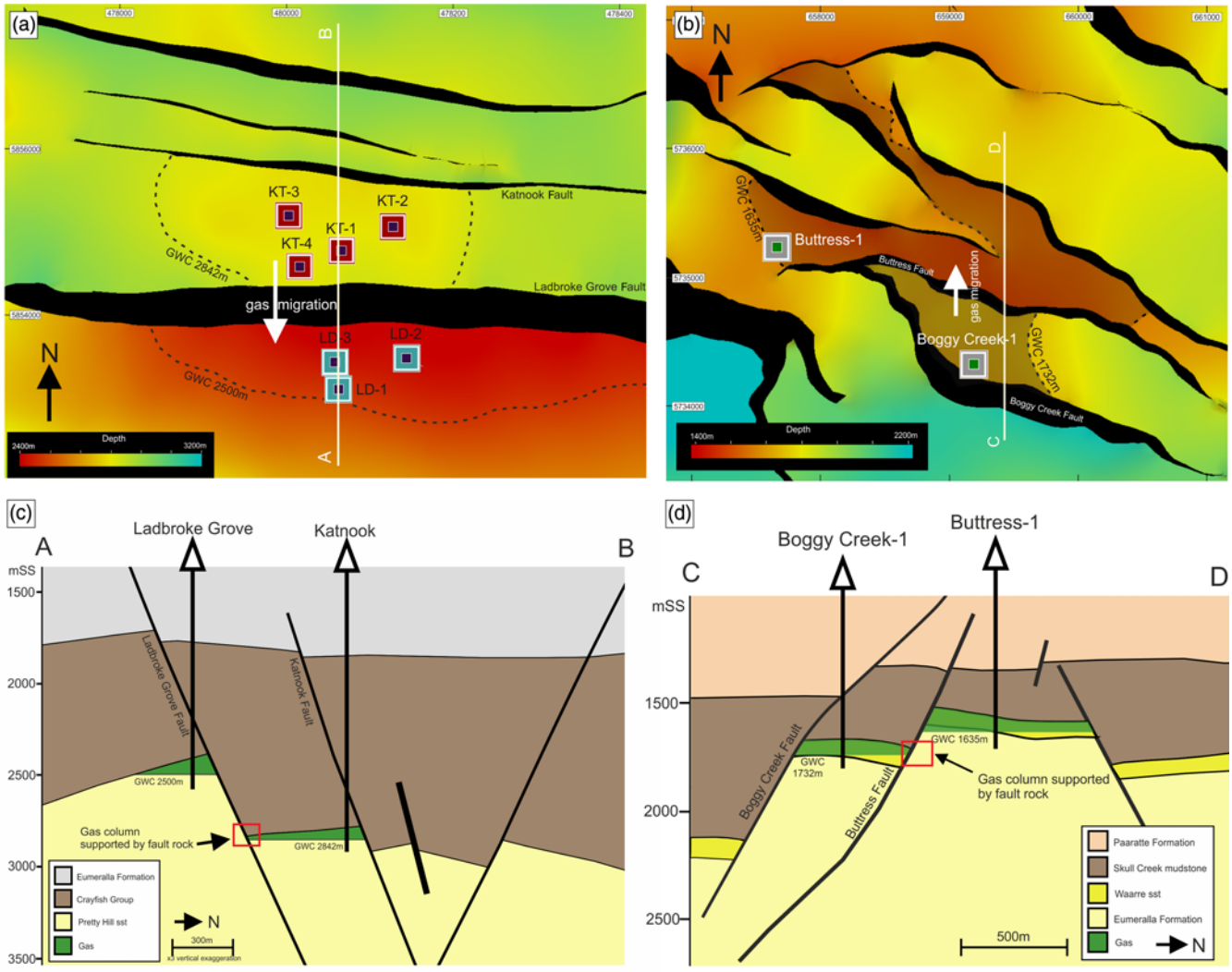

Fig. 2. Map and cross-sectional views of the (**a**) & (**c**) Penola Trough and (**b**) & (**d**) Port Campbell gas field locations. (**a**) Map view of the top of the Pretty Hill reservoir horizon, coloured by depth. (**b**) Map view of the top of the Waarre Sandstone reservoir horizon, coloured by depth. (**c**) Cross-section view of line A–B from (a). The Ladbroke Grove and Katnook fields in the Penola Trough. The cross-section is drawn from seismic data using ×3 vertical exaggeration. The Katnook Field is supported by the Katnook Fault to the north (juxtaposition seal) and the Ladbroke Grove Fault to the south (fault rock seal). (**d**) C–D cross-section view (from b) of the Boggy Creek and Buttress fields in Port Campbell. The cross-section is drawn from seismic data without vertical exaggeration. The Boggy Creek gas field is retained by juxtaposition seal to the south and fault rock seal to the north. The adjacent Buttress Field is structurally higher. The cross-sections were created using the 3D Balnaves–Haselgrove seismic survey (Lyon *et al.* 2004) (c), and a combination of OGF93A, ONH01 and Curdie Vale 3D seismic surveys (Ziesch *et al.* 2017) (d).

a later-stage magmatic CO_2 injection (Chivas *et al.* 1987; Watson *et al.* 2003; Lyon *et al.* 2005*b*). Due to the sealing or partially sealing nature of bounding faults, the CO_2/methane ratio significantly varies across geographically closely located fields.

The Ladbroke Grove Field contains CO_2, with higher concentrations at the base (49%) and lower concentrations at the top of the reservoir interval (27%). The Katnook Field contains primarily methane with only trace amounts of CO_2 (0.2%). $^3He/^4He$, $CO_2/^3He$ and neon isotopic ratios indicate that CO_2 in Ladbroke Grove is of mantle origin ($^3He/^4He = 1.46$ R/R_A, where R is the sample value and $R_A = {}^3He/{}^4He$ in air) (Karolytė 2018). $^3He/^4He$ ratios in the Katnook Field are slightly elevated above the crustal values (0.06 R/R_A) but any mantle-sourced noble gases are decoupled from the migrating CO_2 (Karolytė 2018). The geochemistry results suggest that CO_2 charge was restricted to the Ladbroke Grove Field and did not pass through the Katnook Field. The spill point in the Katnook Field would lead to charging the Balnaves trap, which does not contain a live column (Lyon *et al.* 2005*a*). The presence of a fault-rock-supported column and column absence in the Balnaves Field suggest that methane was likely to have been charged to the Ladbroke Grove Field through failure of fault capillary seal; however, separate charge events cannot be discounted.

The Boggy Creek and Buttress fields both contain mixtures of mantle CO_2 and methane. CO_2 concentrations within the traps increase with depth because of its higher density, and Boggy Creek (87% CO_2) is more CO_2-rich than Buttress (77% CO_2) (Karolytė *et al.* 2019). The observed concentration gradient suggests that CO_2 was first charged to the Boggy Creek Field and later migrated to Buttress, and more methane at the top of the formation was lost relative to CO_2; however, independent charge to both fields cannot be completely excluded.

Methods

Geological 3D models

This work has been undertaken using a compilation of existing industry and academic datasets. 3D model development, and structural and fault seal analysis was undertaken using TrapTester™ software. The Penola Trough 3D model was developed by Paul

Lyon and published in Lyon *et al.* (2004, 2005*b*, 2007). It was constructed by interpretation of the 3D Balnaves–Haselgrove seismic survey in time and pseudo-depth (Lyon *et al.* 2004). The 3D model used for Port Campbell area was developed by Ziesch *et al.* (2017) using a combination of OGF93A, ONH01 and Curdie Vale 3D seismic surveys. Seismic data reinterpretation in this study has led to the addition of some new faults and a modification of fault and horizon geometries in the original models.

V*shale*

The V_{shale} curves for the studied wells were created from gamma-ray (GR) wireline logs. 'Clean sand' and 'pure shale' (0 and 100% V_{shale}, respectively) values were determined by correlating GR measurements to core descriptions and, where possible, core permeability tests from the well completion reports. The Waarre Sandstone is feldspathic (Watson *et al.* 2003), which is reflected in the relatively high chosen density (° API: American Petroleum Institute unit) values of clean sands. The strength of the GR signal is often not uniform between different wells, in which case different clean sand and pure shale values have to be chosen to produce internally consistent V_{shale} logs. The V_{shale} values were calculated using the linear response equation (Asquith *et al.* 2004):

$$V_{shale} = I_{GR} = \frac{GR_{log} - GR_{sand}}{GR_{shale} - GR_{sand}} \quad (3)$$

where I_{GR} is the intensity of the gamma ray log, subscripts sand and shale denote selected representative values for pure shale and sand end–members. Multiple V_{shale} curves were used to project an average V_{shale} profile on the fault plane. Six well logs were used on the Ladbroke Grove fault (LD-1, LD-2, LD-3, JT-1, KT-2 and KT-3) and two on the Buttress Fault (Buttress-1 and Boggy Creek-1).

Fault seal modelling

The intersection lines between the top of the reservoir formation on the footwall and the hanging-wall sides of the fault were created on the fault planes (e.g. Yielding and Freeman 2016). Manual quality-check techniques, such as projecting seismic slices on the fault plane, were used to accurately map out the geometry of the intersections. Allan diagrams (Allan 1989) were created to identify the areas of interest where reservoir formation is juxtaposed against another permeable rock on the other side of the fault.

Buoyancy pressure is calculated on the 3D surface of the fault based on the input of GWC and gas pressure gradient (see Supplementary material 1), which is dependent on the fluid density. Gas densities at reservoir conditions for the particular gas mixtures were calculated using the Peng–Robinson equation of state (Peng and Robinson 1976). The pressure data were obtained from repeat formation tester (RFT) plots in well completion reports (WCRs) from the Buttress and Ladbroke Grove fields. Pressure profile data did not exist for Katnook and Boggy Creek fields, so gas pressure gradients were calculated from gas densities. A summary of input parameters relevant to buoyancy pressure calculation is given in Table 1.

SGR was calculated on the 3D plane of the fault using the input of V_{shale} curves using the Yielding *et al.* (1997) method. The threshold capillary pressures were calculated using two different SGR calibration techniques: empirical (Yielding 2002; Yielding *et al.* 2010) and deterministic (Sperrevik *et al.* 2002) (detailed methods are available in Supplementary material 1). Both of these methods require an input of the maximum burial depth. The empirical method uses the burial depth to categorize faults for three different seal envelopes (<3, 3–3.5 and 3.5–5 km), while the deterministic method directly incorporates the value. The deterministic method additionally requires an estimate of the depth at the time of faulting and a conversion factor from a mercury–air to a gas–brine system, which is dependent on the interfacial tension between the wetting and non-wetting phases and the wettability of the system. A minimum and maximum estimate of each of the parameters were determined based on known reservoir conditions and a literature review, resulting in two and eight possible scenarios for the empirical and deterministic methods, respectively (Fig. 3). Both of these methods ascribe threshold capillary pressures to every point of the 3D fault surface. These can then be compared to the known buoyancy pressure exerted by the gas column trapped in the reservoir.

Input parameters

The input parameters used in the fault seal modelling are summarized in Table 2, and the reasoning is explained in the following subsections.

Maximum burial depth. The Otway Basin has undergone two significant phases of uplift and denudation but the effects are less significant at the margins of the basin where the two case studies are situated. A comprehensive basin-wide sonic transit time study by Tassone *et al.* (2014) suggests that Port Campbell is close to its maximum burial depth, with a net exhumation range obtained from Boggy Creek-1 indicating 0–160 m net exhumation. The same is true for Penola Trough, where a conservative estimate of net exhumation is in the range of 0–200 m. This is confirmed by vitrinite reflectance and apatite fission-track data (Duddy 1997; Boult and Hibburt 2002). The upper end of this range gives a maximum burial depth of 2987 m, which is very close to the cut-off value of 3 km between different seal envelopes in the Yielding *et al.* (2010) method. We therefore consider two scenarios of <3 and 3–3.5 km maximum burial depth for the Penola Trough.

Depth at the time of faulting.

- Penola Trough – the main faulting event was contemporaneous with the Early Cretaceous rifting that coincided with

Table 1. *Summary of parameters used in the buoyancy pressure calculations*

Field	Temperature (°C)	Pressure (MPa)	GWC (m subsea)	ρ_w (kg m^{-3})	ρ_g (kg m^{-3})	Major gas composition		
						C_1+	N_2	CO_2
Penola Trough								
Ladbroke	104	23	2500	927	244	45	7.2	49
Grove								
Katnook	118	28	2842	1035	125	97	3.2	0.2
Port Campbell								
Buttress	62	16	1635	1035	382	22	1.9	77
Boggy Creek	59	17	1732	1035	456	10	2.0	87

Temperature and pressure are relevant where density was calculated using an equation of state rather than obtained from RFT measurements. Major gas compositions are from Karolytė (2018) and Karolytė *et al.* (2019).

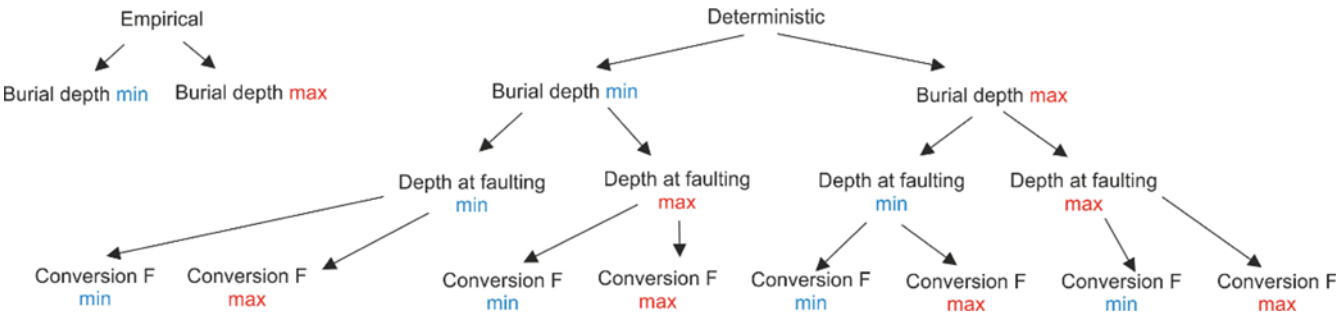

Fig. 3. Schematic diagram of different scenarios including minimum and maximum estimates of parameters required by the empirical and deterministic methods.

the deposition of the regional seal formation. The sediments of the Crayfish Group commonly drape over major structural highs, indicating that faulting had ceased by the end of its deposition (Briguglio *et al.* 2015) and was inactive during the deposition of the overlying Eumeralla Formation (Boult *et al.* 2008), which is also evident from the seismic data. The depth of Ladbroke Grove Fault at the time of displacement is therefore constrained by the total thickness of the Crayfish Group. The current thickness of the Crayfish Group in the Katnook well is 800 m, which is also the thickest in the Penola Graben. Structural cross-section balance and restoration indicates that 400 m of Crayfish sediments were removed in the Penola Graben (Briguglio *et al.* 2015). Depth at the time of faulting is therefore constrained to 800–1200 m.

- Port Campbell – the seal formation, consisting of a succession of mudstones overlain by Skull Creek mudstone, varies in thickness across the faults, indicating synsedimentary faulting (Ziesch *et al.* 2015). The faulting ceased during the deposition of the unconformably overlain Wangerrip Group in the Paleocene. Depth at the time of faulting is therefore represented by the thickness of this group, which ranges from 450 to 1200 m.

Conversion factor

The conversion factor from mercury–air to the chosen wetting and non-wetting phase requires an input of IFT and CA:

$$P_{wn} = P_{ma}\,\frac{\mathrm{IFT}_{wn}\cos\theta_{wn}}{\mathrm{IFT}_{ma}\cos\theta_{ma}} \quad (4)$$

where P is threshold capillary pressure, θ is the contact angle, and the subscripts wn and ma denote the wetting/non-wetting phase of choice and mercury–air, respectively. The air–mercury IFT and CA are 480 mN m^{-1} and 140°, respectively (Vavra *et al.* 1992).

IFT has a strong dependency on pressure and temperature for both CO_2 and methane, so assessment for local reservoir conditions is imperative. Figure 4 shows a compilation of results selected from laboratory studies under conditions similar to those in the Boggy Creek and Katnook reservoirs. Presented data include CH_4–water, CO_2–water, CO_2–brine and CO_2–CH_4 mixtures in water (Hough *et al.* 1951; Wiegand and Franck 1994; Tian *et al.* 1997; Ren *et al.* 2000; Chalbaud *et al.* 2009; Georgiadis *et al.* 2010; Kashefi 2012). The range constrained for the Boggy Creek Field is 26–32 mN m^{-1} (Fig. 4). Admixture of CH_4 to pure CO_2 generally increases the IFT but, as shown in Figure 4a, the measurements in mixtures containing <20% methane are not significantly different from the CO_2–water system (Ren *et al.* 2000). The IFT range expected in the Katnook methane field is 47–49 mN m^{-1} (Fig. 4b).

Typical reservoir rocks are often considered to be water-wet in the presence of hydrocarbons (e.g. Schowalter 1974; Vavra *et al.* 1992), with some exceptions, including grain coating with high polarity of crude oil components (Singh *et al.* 2016). The Penola Trough traps show evidence for early charge of oil which was later displaced by gas (Lovibond *et al.* 1995; Higgs *et al.* 2015); therefore, a range in CA of 0°–30° is taken to reflect the potential effect of acid adsorption on grain surfaces.

The wettability of a CO_2–brine–mineral system has been investigated by a growing number of studies (Bikkina 2011; Jung and Wan 2012; Farokhpoor *et al.* 2013), most commonly directly on single mineral surfaces, where minerals are required to be ultraclean and smooth on an atomic level for reproducible results. The results are highly variable (0°–90°) but much of the variation is attributed to the surface roughness and sample preparation practices (Iglauer *et al.* 2015). However, the most consistent findings include an increase in CA by up to 30° at the CO_2 transition from the gaseous to the supercritical phase (Sutjiadi-Sia *et al.* 2008; Jung and Wan 2012). Recent core-flooding experiments show that water-wet reservoir conditions do not change during prolonged exposure to supercritical CO_2 (Garing and Benson 2019). In the absence of minerals known to be particularly hydrophobic in the presence of CO_2 in the reservoir, the expected CA range for Boggy Creek is taken to be 10°–40°, as expected for common silicate and carbonate reservoir minerals (Espinoza and Santamarina 2010).

Given the defined range of IFT and CA for both reservoirs, minimum and maximum conversion factors calculated for Boggy Creek Field (CO_2-dominated) and Katnook Field (methane-dominated) were 0.054–0.087 and 0.111–0.133, respectively.

Results

Structural and fault rock composition results

The Allan diagrams in Figure 5 show the juxtaposition of lithologies along the strike of the fault planes for the Katnook (Fig. 5a) and

Table 2. *Summary of the parameters used in fault seal modelling*

	Burial depth (m) (for deterministic)		Burial depth (m) (for empirical)		Depth at the time of faulting (m)		Conversion factor	
Field	Minimum	Maximum	Minimum	Maximum	Minimum	Maximum	Minimum	Maximum
Boggy Creek	1623	1783	<3000	–	450	1200	0.054	0.087
Katnook	2787	2987	<3000	3000–3500	800	1200	0.111	0.133

Boggy Creek (Fig. 5b) reservoirs. The Katnook reservoir is primarily sealed by sand–shale juxtaposition by the Katnook Fault to the north but the field extends to the hanging wall of the Ladbroke Grove Fault which is supporting the column to the south (Fig. 5a). The entire extent of the reservoir is juxtaposed against reservoir on the other side of the fault. Similarly, the Boggy Creek Field is supported by sand–shale juxtaposition in the footwall of the Boggy Creek Fault to the south. The field extends to the hanging wall of the Buttress Fault (Fig. 5b), where the reservoir is self-juxtaposed for the entire extent of the gas field. Calculated V_{shale} values for areas of reservoir self-juxtaposition range between 20 and 50% on the Ladbroke Grove Fault, and from 10 to 80% on the Buttress Fault. In the reservoir interval, SGR values range from 35 to 41% on Ladbroke Grove Fault and from 60 to 70% on the Buttress Fault (Fig. 6). SGR values above 20% are considered to be sealing (Yielding *et al.* 2010), so in both cases the model indicates that the faults are acting as barriers to gas migration.

Threshold capillary pressure

Across-fault leakage through capillary seal breach commonly occurs where the lowest SGR values coincide with the highest buoyancy pressure on a given fault plane. In the two cases discussed here, the highest points of the trap correlate with the lowest SGR values, making the top of the fault the most likely to leak (Fig. 7). The buoyancy pressure values identified at these points are 0.28 MPa for the Katnook Field and 0.29 MPa for the Boggy Creek Field.

The calculated threshold capillary and buoyancy pressures can then be compared at the critical points, where the difference between them represents the amount of extra pressure (or extra gas column) the fault can retain before seal breach. Figure 8 shows the results of the deterministic (Fig. 8a and c) and empirical (Fig. 8b and d) calibrations for the Ladbroke Grove Fault in the Katnook Field, and the Buttress Fault in the Boggy Creek Field.

The results from both calibrations for the Katnook methane gas field indicate that the current live gas column of 31 m (equivalent to 0.28 MPa buoyancy pressure) is stable but the fault is close to capillary seal breach. The threshold capillary pressures range from 0.32 to 0.55 MPa, equivalent to a total column of gas of between 35 and 57 m according to the deterministic calibration. Empirical calibration suggests that the fault seal will be breached at pressures of between 0.3 and 0.57 MPa, equivalent to a total gas column of 33–63 m. The results from both calibrations are remarkably similar, with an average threshold capillary pressure of 0.42 and 0.43 MPa using the deterministic and empirical methods, respectively.

The deterministic and empirical methods provide different results for the Boggy Creek CO_2 field. The fault is currently supporting a 51 m column of gas, equivalent to a buoyancy pressure of 0.29 MPa. This is close to the upper-range values predicted by the deterministic method. The threshold capillary pressure ranges from 0.15 to 0.31 MPa (26–55 m of total column height). The predicted average column height is 39 m, slightly underpredicting the sealing potential of the fault. In contrast, the empirical calibration indicates a threshold pressure of 0.65 MPa and a maximum column height of 115 m, which is more than double the current amount.

The empirical method requires only one parameter of the maximum burial depth; the deterministic method requires three parameters. In the case of the Katnook methane field, the uncertainty in maximum burial depth has the biggest impact on the results and the conversion factor is the second largest uncertainty (see the *y*-axis annotation in Fig. 8). In contrast, the uncertainty in the conversion factor has a greater impact on the Boggy Creek CO_2 field results than the maximum burial depth.

The structural spill point at the Katnook Field is identified at 2891 m, which effectively allows a maximum gas column height of 81 m. In Boggy Creek, the structural spill point occurs at 1956 m, allowing a maximum column height of 272 m. The maximum column heights identified from the structural perspective of the traps are all higher than those modelled by fault seal analysis. This means that filling the traps to the maximum fault rock threshold pressures derived from all models would not result in fill-to-spill and therefore both methods indicate that migration to the adjacent fault trap occurred through the fault rather than through over-spilling.

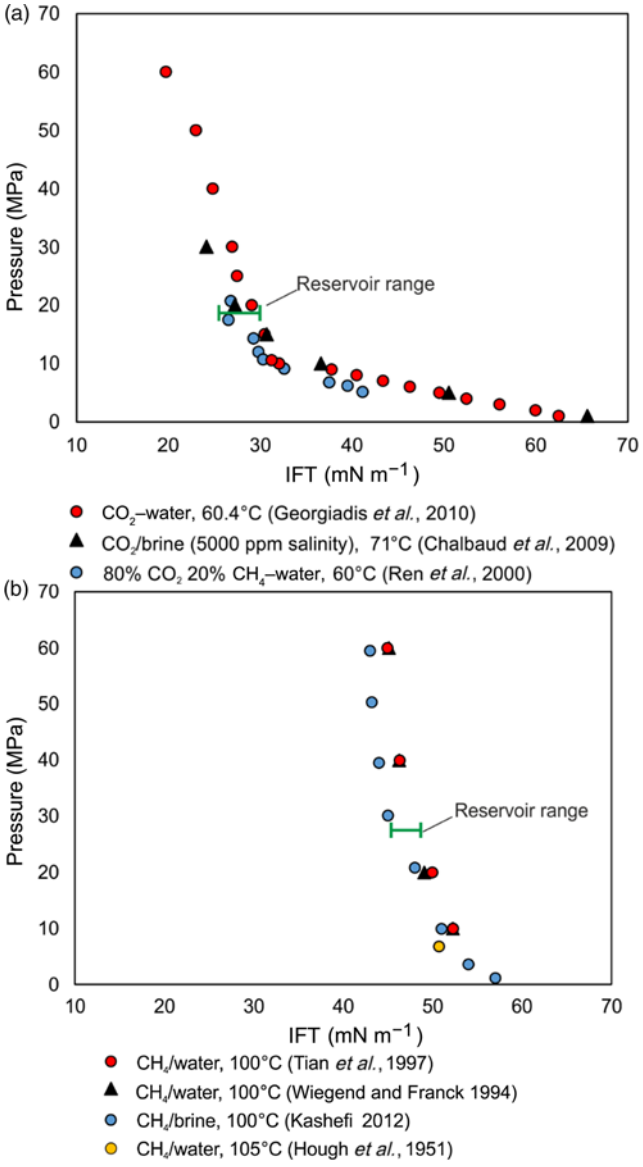

Fig. 4. IFT v. pressure for (**a**) Boggy Creek reservoir conditions and (**b**) Katnook reservoir conditions. The green line shows the expected range for reservoir pressure.

Discussion

Addressing the uncertainty in fault seal modelling

The deterministic and empirical methods present a key difference in their definition of the threshold capillary pressure. The deterministic method defines a best-fit line through the data points of measured capillary entry pressures during injection experiments to fault rock samples. Therefore, by definition, the method predicts the average threshold pressure for the modelled conditions. In contrast, the fault seal envelopes defining the threshold capillary pressure in the empirical method represent the upper limit of data for buoyancy

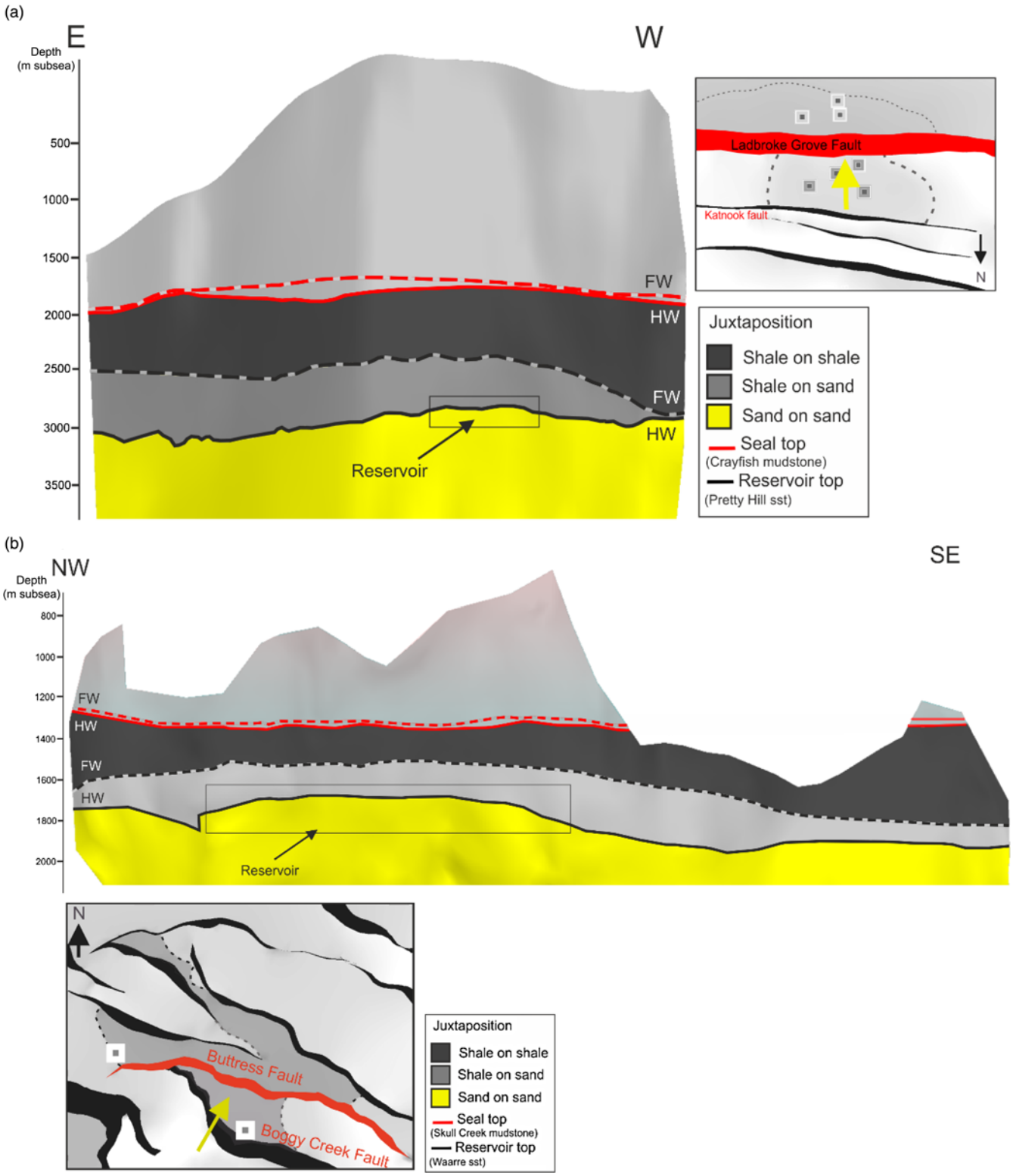

Fig. 5. Allan diagrams showing juxtaposition along the strike-view of the faults, viewed from the hanging-wall side. Insets show the location of the faults (marked in red), the yellow arrows show the direction of view. (**a**) Ladbroke Grove Fault, supporting the southern side of the Katnook gas field (×3 vertical exaggeration). (**b**) Buttress Fault, supporting the northern side of the Boggy Creek gas field (no vertical exaggeration). Black rectangles show the extent of the gas-bearing reservoir. Horizon intersections on the fault plane are displayed as dashed lines for the footwall side and solid lines for the hanging-wall side.

pressures retained by fault rocks with a given SGR. The threshold pressure returned by the empirical equation is therefore a maximum estimate. In other words, even though the same term of threshold capillary pressure is used by the two methods, the derived value represents somewhat different concepts and presents a different level of uncertainty.

Some uncertainties are inherent to the modelling method and cannot be easily accounted for. The deterministic method is based on threshold capillary pressure measurements of microfault samples on the scale of millimetres to centimetres (Sperrevik *et al.* 2002). The measured clay content of the fault structures is assumed to be represented by SGR when upscaled to use in a predictive way. The

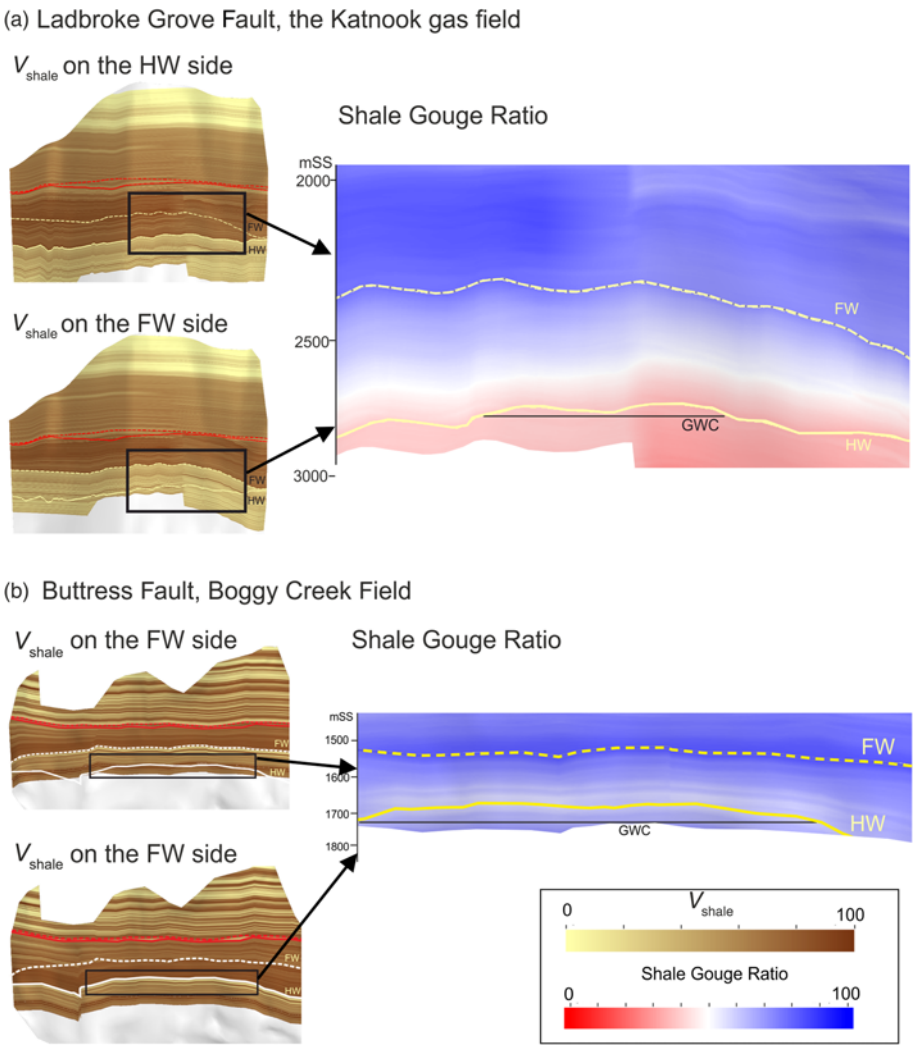

Fig. 6. Composite V_{shale} curves projected on the hanging wall (HW) and footwall (FW) of the fault plane and the calculated SGR values. (**a**) The Ladbroke Grove Fault; SGR range 35–41%. (**b**) The Buttress Fault; SGR range 60–70%.

method is therefore applied on the assumption that kilometre-scale faults behave in the same way as microstructures. In reality, this is not strictly the case, with seismic-scale fault zones comprising clay smears, cataclastic zones and multiple planes of deformation (Fisher and Knipe 1998; Shipton and Cowie 2001; Faulkner *et al.* 2010; Pei *et al.* 2015; Bense *et al.* 2016), which all add to the total sealing capacity of the fault zone. Detailed fault zone analyses show that the permeability over individual fault zone components can vary considerably (e.g. over three orders of magnitude) (Shipton *et al.* 2002) and therefore upscaling one of those components to be

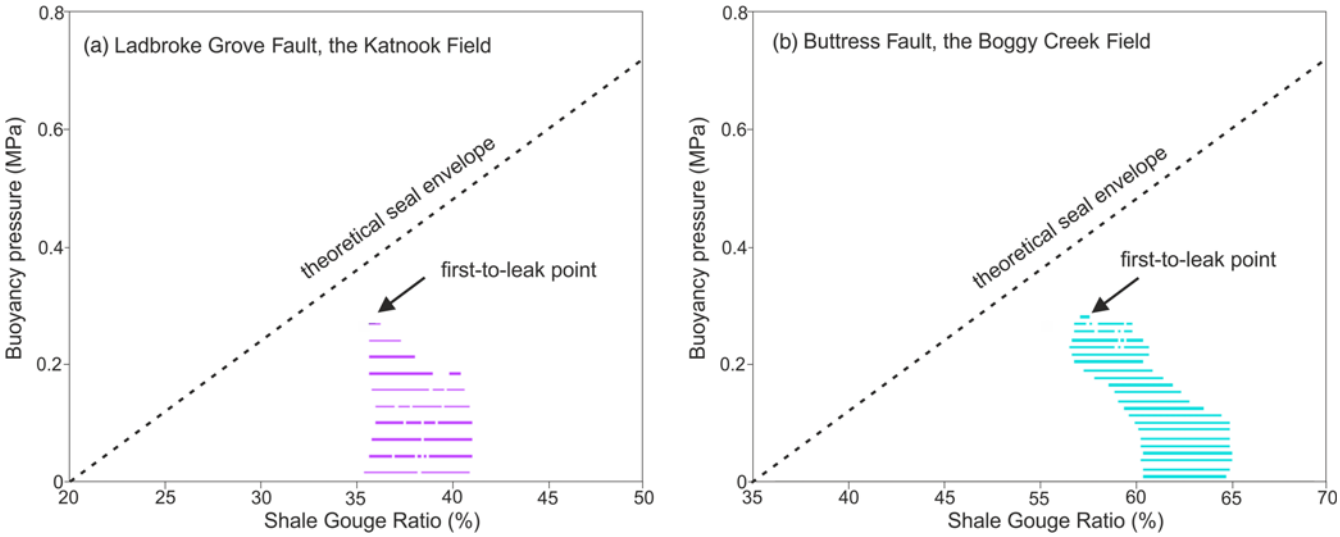

Fig. 7. Buoyancy pressure v. SGR calculated for every point of the 3D fault plane within the gas column for (**a**) the Katnook methane field, Penola Trough and (**b**) the Boggy Creek CO_2 field, Port Campbell. The first-to-leak points in both cases occur where the highest buoyancy pressure coincides with the lowest SGR values (black arrow), which happens to be at the top of the gas fields. The dashed line shows a theoretical seal envelope line. The first-to-leak point is always closest to the seal envelope line.

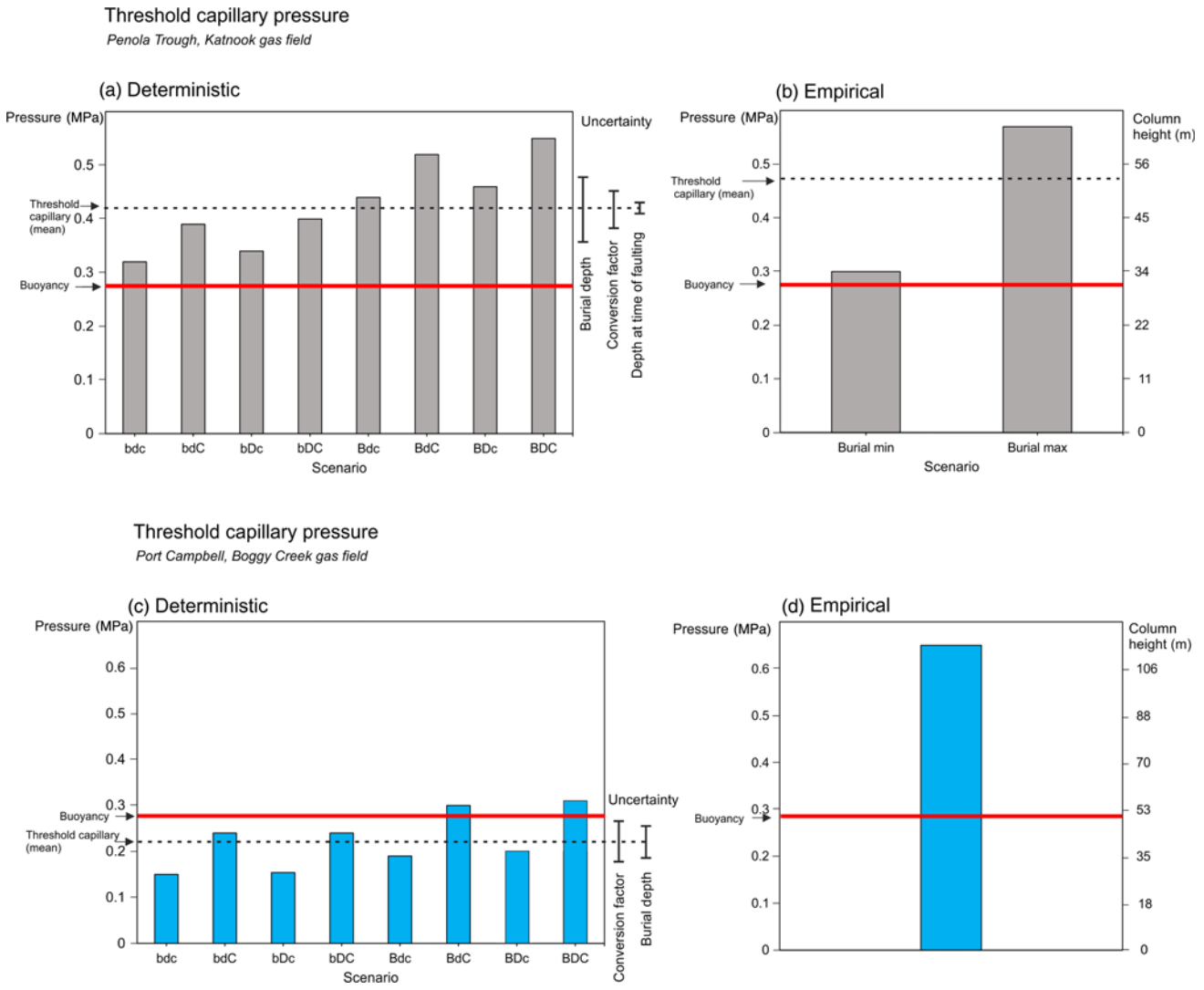

Fig. 8. Bar chart showing the threshold capillary pressure results for (**a**) & (**b**) the Katnook methane field and (**c**) & (**d**) the Boggy Creek CO_2 field using deterministic (a & c) and empirical (b & d) SGR calibration algorithms. Conversion to column height is displayed on the secondary *y*-axis (same values applicable to both deterministic and empirical method graphs). The red line shows the current column height/buoyancy pressure. The Katnook gas column is predicted to be stable by both methods, with maximum threshold capillary pressure ranging from 0.32 to 0.55 MPa (deterministic) and from 0.3 to 0.57 MPa (empirical). The Boggy Creek Field is predicted to be within the upper end of the critical pressure zone by the deterministic method (0.15–0.31 MPa) and stable by the empirical method. Labels in deterministic scenarios: B, maximum burial depth; D, depth at the time of faulting; C, conversion factor. Upper and lower case letters indicate maximum and minimum values, respectively.

representative of the entire fault zone involves a significant simplification.

The advantage of the empirical method in this respect is that SGR is assumed to be a proxy for the fault sealing properties, which include shale content but also various heterogeneous components of the fault zone. SGR calculated on the 3D surface of the fault planes is the direct input into the calibration as well as in the predictive workflow, which eliminates the uncertainty associated with equating SGR to specific rock properties such as the true volume of shale. The compilation dataset includes data from seven different basins, covering a wider range of diagenetic conditions relative to the deterministic method which is based on samples from the North Sea (Yielding 2002).

Some of the uncertainties associated with the local geological conditions and fluid properties are parameterized in the deterministic method and therefore can be accounted for. The error bars in Figure 8a and c show the relative uncertainties associated with the different model input parameters. For the two case studies presented here, fluid properties (governing the conversion factor) present a higher uncertainty for CO_2 rather than methane. This is primarily due to the larger IFT range selected for CO_2 but does not suggest that the interfacial tension of CO_2 is less characterized than that of methane. The larger range is due to a relatively higher number of currently available studies, including measurements using different salinity, salt types and gas mixtures, while methane laboratory studies are largely constrained to pure methane and deionized water. In cases where fluid properties are well defined, maximum burial depth is the most significant source of uncertainty, while depth at the time of faulting is the least significant input parameter.

Uncertainty related to fluid properties

An important difference between the two methods is the approach to accounting for the fluid properties. The IFT and wettability are parameterized in the deterministic method, making it more versatile, arguably adaptive, to a CO_2–brine system and more precise in cases where fluid properties are well characterized. The empirical method does not explicitly address the fluid properties but operates under the assumption that the range of IFT and CA configurations in hydrocarbons is small, and that the possible variability of fluid properties is represented in the global dataset compilation. The two important issues with the empirical approach are:

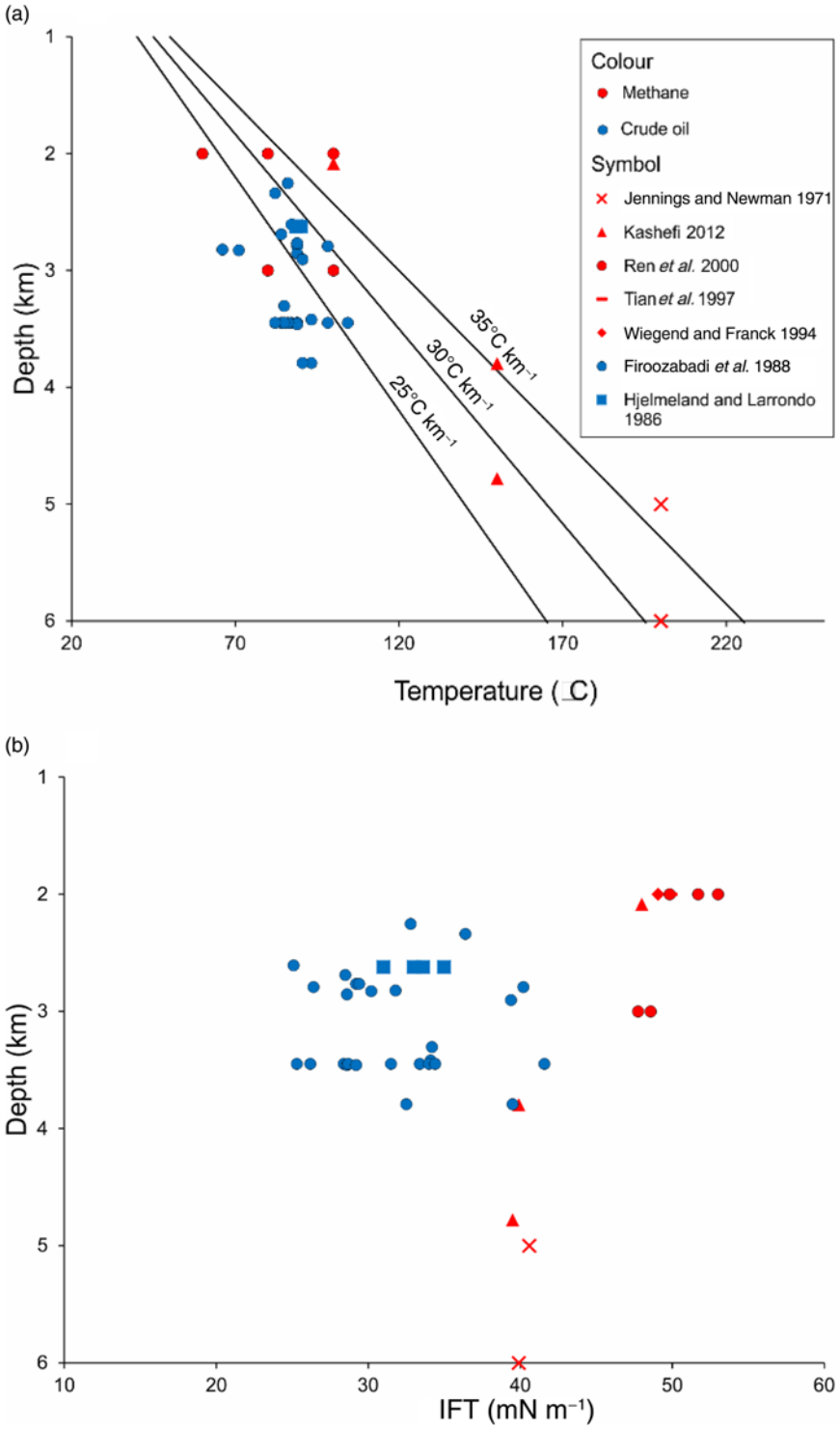

Fig. 9. IFTs of crude oil and methane data compiled from the literature, filtered to conditions applicable to geological pressure and temperature conditions (25–35 °C km^{-1} geothermal gradient). (**a**) shows the distribution depth v. temperature conditions. (**b**) shows the IFT values of the same data points. Crude oil IFT values range between 26 and 42 mN m^{-1}, and are uniformly distributed. Methane values range between 40 and 53 mN m^{-1} and decrease with depth. Combined together, these data represent a uniform distribution. Full data set available in Supplementary Material 2.

- The uncertainty related to fluid properties is undefined when applied to hydrocarbons.
- The application to CO_2 can only be considered valid in cases where CO_2 exhibits properties within the range of those observed in hydrocarbons.

These are explained in detail in the following subsections.

Uncertainty related to fluid properties of hydrocarbons in the empirical model

To further assess the empirical method application to CO_2, the uncertainty related to the fluid properties of hydrocarbons has to be defined. The percentage error of the capillary threshold pressure (δP_c) from the uncertainty in fluid properties (as a standard deviation) can therefore be expressed as, using equation (1):

$$\delta P_c = \frac{\sigma(P_c)}{\mu(P_c)} \times 100\% = \frac{\sigma(2\text{IFT}\ \cos\theta)}{\mu(2\text{IFT}\ \cos\theta)} \times 100\% \qquad (5)$$

where σ is the standard deviation and μ is the average value of the probability distribution. The empirical method uses a data compilation including both oil and methane in reservoirs of >1.5 km in depth (Yielding 2002), and can be assumed to reflect the general IFT and CA variability of all hydrocarbons at that depth. The percentage error can therefore be calculated using a random sampling modelling approach with inputs of the probability distribution of IFT and CA values in a hydrocarbons–brine

system. Theoretically, the CA is related to the IFT at the interfaces between the solid and the fluids based on the Young's equation; however, the solid–fluid interface presents significant variability based on the type of solid. A significant number of factors affecting the CA not directly related to the fluid type exist. We therefore assume the IFT and the CA to be independent variables.

Defining IFT and wettability range for hydrocarbons

The IFT between hydrocarbons and water (or brine) is primarily controlled by the chemical composition of the hydrocarbons, the density contrast between the two phases and temperature (Hassan *et al.* 1953; Flock *et al.* 1986; Rajayi and Kantzas 2011). Pressure mainly affects gas solubility in oil and therefore has a greater effect on oils with high dissolved gas content (Ghorbani and Mohammadi 2017). Generally, the IFT in hydrocarbons is not well characterized and usually an average IFT of 30–35 mN m^{-1} is used for capillary seal modelling purposes (Berg 1975; Sneider *et al.* 1997). Considerable effort has been made to characterize the IFT of individual hydrocarbon compounds, and to derive predictive equations to determine the IFT based on the input of reservoir temperature (Kalantari Meybodi *et al.* 2016), density difference (Danesh 1998; Sutton 2006) and critical fluid temperature (Najafi-Marghmaleki *et al.* 2016). However, these methods are developed for data compilations of pure aromatics and alkanes, and do not reflect the fluid properties of crude oil at reservoir conditions, which include a high percentage of other compounds such as napthenes and asphaltics (Buckley *et al.* 1997).

There have been relatively few studies presenting IFT measurements in crude oil–water systems but these can be considered the most reservoir-representative. Figure 9 shows a compilation of laboratory measurements within the envelope of pressures and temperatures valid for geothermal gradients between 25 and 35°C km^{-1}, and hydrostatic pressure gradient of 10 MPa km^{-1}. The compilation includes samples of crude oil above bubble point representing non-degassed oils, and below-bubble point oils and methane. The IFT values of crude oil are in the range 26–42 mN m^{-1} and are more strongly controlled by chemical differences rather than depth. The IFT of methane decreases with depth and ranges between 40 and 53 mN m^{-1}. Based on this example dataset, it is assumed that the IFT values of hydrocarbons used in the empirical calibration method are expected to be within a uniform probability distribution with a mean value of 39 ± 8 mN m^{-1} (Fig. 10a).

In the context of capillary seal modelling, reservoir formations are generally considered to be water-wet in the presence of hydrocarbons (CA = 0°) (e.g. Schowalter 1974; Vavra *et al.* 1992). This is not strictly true with mixed-wet and oil-wet states often observed in hydrocarbon reservoirs (Treiber and Owens 1972), often due to mineral surface coating with high-polarity crude oil components such as asphaltenes which have high affinity to the reservoir minerals (Alipour Tabrizy *et al.* 2011; Singh *et al.* 2016). The degree of oil-wetting is expected to be higher in reservoirs containing high maturity oil, and in the presence of carbonate cements, smectite, chlorite, kaolinite and iron oxides (Worden and Morad 2000; Barclay and Worden 2009). Because the CA directly affects the calculated column heights and associated threshold capillary pressures, the practice of assuming a CA of 0° in hydrocarbon reservoirs always provides a maximum rather than conservative estimate. In the absence of strong statistical data, we assume that reservoir rocks are more commonly water-wet than oil-wet in the presence of hydrocarbons. This spread of data is best described by an exponential probability distribution ($\beta = 15$), with a mean value of 15 ± 15° (Fig. 10b). The lowest values in the range are the most probable. Based on equation (3), retention of a gas column is only possible when the CA is ≤90° ($\cos\theta > 0$). Because the dataset by definition only includes reservoirs with observed columns, the CA must range between 0° and 90°.

Based on the probability distributions of IFT and CA determined above, the percentage error of threshold capillary pressure (δP_c) determined from equation (5) using Monte Carlo random sampling analysis ($n = 10^6$) is 24%. Figure 11 shows the seal failure envelopes of the empirical model (Yielding *et al.* 2010) with the calculated error added. The seal envelopes define the upper boundary of all buoyancy pressures observed to be sealed by fault rocks and therefore statistically represent the higher values within the data distribution or maximum threshold capillary pressure. We can therefore use the calculated percentage error to estimate the average threshold capillary pressure ($P_c - \sigma$) and the minimum threshold capillary pressure ($P_c - 2\sigma$). The uncertainty increases with increasing P_c.

Implications for use in hydrocarbons. The calculated uncertainty envelopes do not change the interpretation of the empirical calibration method but, rather, provide additional constraints that can be applied in a variety of contexts. In cases where capillary pressure modelling is used to assess the economic viability of the reservoir, the uncertainty can be a useful input into the risking process. The average threshold capillary pressure value is better used in the calculation of likely hydrocarbon column heights, bearing in mind that the true column height can be controlled by many factors independent of fault seal, such as structural spill points and charge. In cases where sufficient geological evidence exists to indicate that the trap has been filled, the calculated uncertainty envelope provides means to determine the minimum expected column. The average threshold capillary pressure value using the

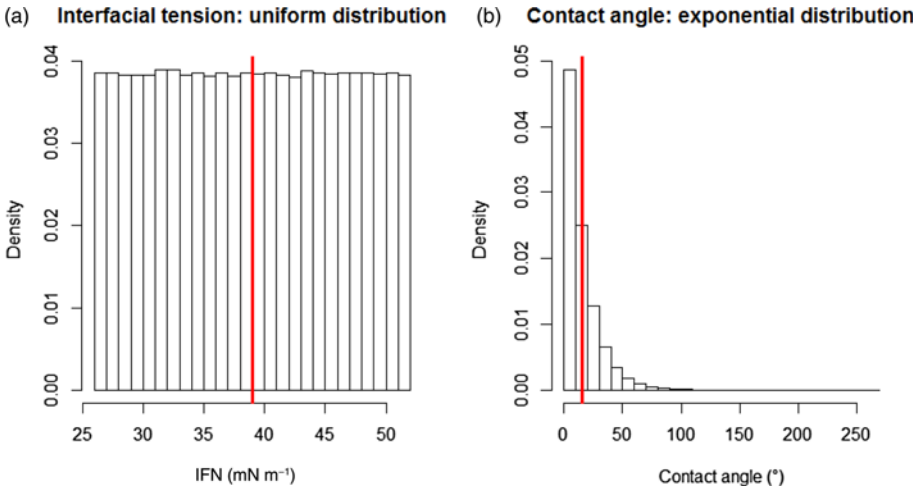

Fig. 10. Probability distribution of (**a**) interfacial tension (IFT) and (**b**) contact angle (CA) in hydrocarbons at reservoir conditions below 2 km depth, defined based on a literature review of laboratory studies (discussed in the text). The red vertical line shows the mean. IFT is expected to be uniformly distributed with a mean value of 39 ± 8 mN m^{-1}. The exponential distribution ($\beta = 15$) best describes the expected CA.

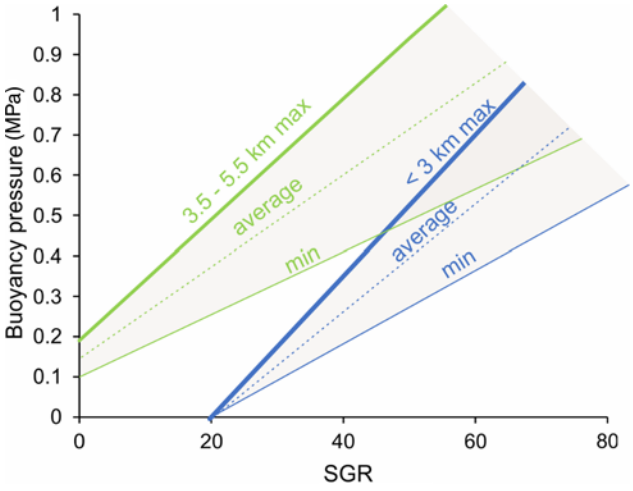

Fig. 11. SGR v. buoyancy pressure with <3 and 3.5–5.5 km threshold capillary pressure envelopes from Yielding *et al.* (2010). The thick solid line shows the original maximum threshold capillary pressure. Dashed line shows the new corrected threshold capillary pressure, which can be seen as the average value. The maximum (thick solid) and minimum (thin solid) lines represent the 24% percent error margins.

empirical method is also more comparable to the average results of the deterministic method (rather than using the current empirical maximum value) when the two are used in conjunction.

Empirical method applied to the fluid properties of CO_2

In the last decade, significant effort has gone into characterizing the IFT of CO_2 at a range of conditions, with existing data covering CO_2–water (Chiquet *et al.* 2007*a*; Georgiadis *et al.* 2010) and CO_2–brine with variable salinity and salt types (Bachu and Bennion 2009; Chalbaud *et al.* 2009). The IFT has been characterized for mixtures of CO_2 and methane in water (Ren *et al.* 2000) and brine (Liu *et al.* 2016). Increasing brine salinity has been shown to increase the IFT in a CO_2–brine system with significant deviations in saline and hypersaline conditions (Bachu and Bennion 2009; Chalbaud *et al.* 2009; Liu *et al.* 2016). Figure 12 shows results from published laboratory studies filtered to those that are representative of pressure and temperature conditions in the subsurface (geothermal gradients of 25–35°C km^{-1} and hydrostatic pressure gradient of 10 MPa km^{-1}). The data include pressures above 15 MPa (*c.* 1.5 km depth), which is in line with depths recommended for safe geological CO_2 sequestration (>1.2 km) (Miocic *et al.* 2016). It is apparent that in the supercritical fluid state, depth does not significantly influence the IFT. The most important controlling factor is brine salinity which increases the IFT due to an increasing density contrast between CO_2 and the brine. The maximum IFT values of 44.7 and 41.1 mN m^{-1} at 1.7 and 2.7 km depth, respectively, from the study of Bachu and Bennion (2009) are measured in brines of 334 g l^{-1} salinity, which is close to the maximum possible salt saturation in water. In comparison, the salinity of UK oil and gas fields ranges from 30 to 227 g l^{-1}, with an average value of 130 g l^{-1} (Gluyas and Hichens 2003). The IFT range presented here covers the minimum (CO_2–pure water) to maximum (CO_2–hypersaline brine) geologically possible conditions relevant to a CO_2 sequestration context (>1.5 km depth), and also falls within the range observed in liquid hydrocarbons. The IFT values range between 26 and 45 mN m^{-1}, which is remarkably similar to the IFT range in crude oil (26–42 mN m^{-1}: Fig. 9).

The wettability in a CO_2–brine system is a complex issue and cannot be easily defined as a bracket range for all reservoir conditions. The conditions of many experimental set-ups are very different to reservoir conditions, as discussed in the earlier

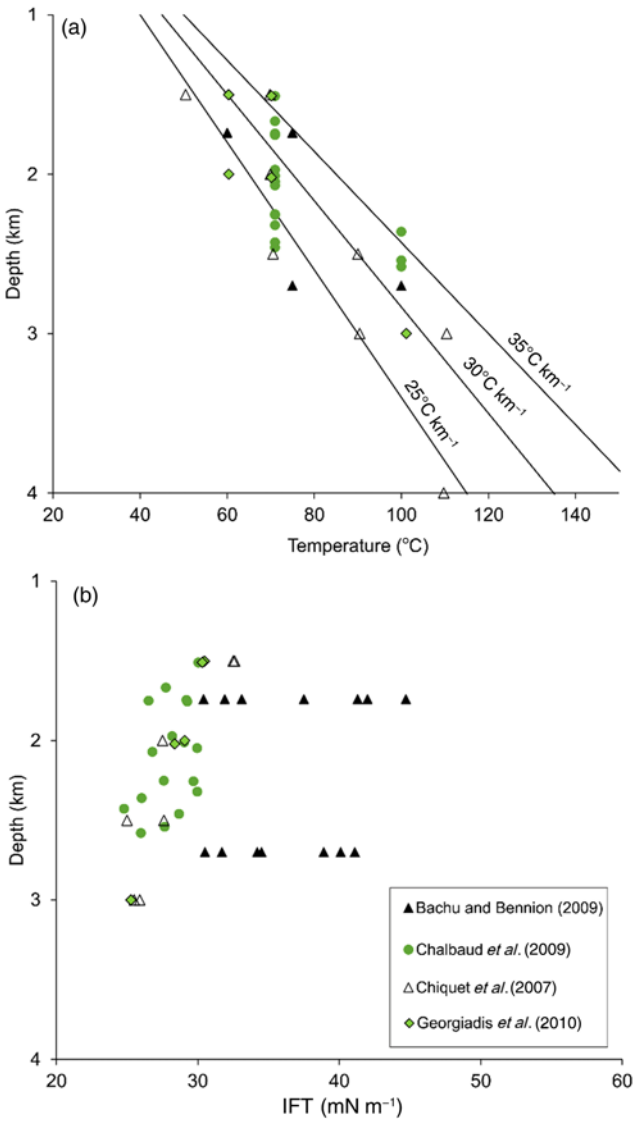

Fig. 12. IFT of CO_2 in water and brine of different salinities, filtered to only display pressure and temperature conditions applicable to geological setting (25–35°C km^{-1} geothermal gradient). (**a**) shows the distribution depth v. temperature conditions. (**b**) shows the IFT values of the same data points. IFT ranges from 26 to 45 mN m^{-1}. Data points from Bachu and Bennion (2009) show the effects of increasing salinity, with a maximum of 334 g l^{-1} resulting in the highest IFT values. Full data set available in Supplementary Material 2.

'Conversion factor' subsection; therefore, the upscaling of single mineral experimental results to reservoir is problematic. Irrespective of this variation, the most significant observation emerging from CO_2–brine laboratory studies is the change in wettability caused by pressure. This is observed when CO_2 changes from the gaseous to supercritical fluid phase at around 8 MPa. It is presently not understood if the change in wettability is related to the process of phase change or to the physical properties of supercritical CO_2. Single-mineral studies reveal that CAs are significantly higher in the presence of physosilicate minerals relative to quartz; this effect increases with pressure and temperature (Arif *et al.* 2016). This could mean that an increasing clay fraction in the fault rock, which correlates with an increasing SGR, may also have an opposing negative effect to the overall sealing potential of the rock. The important step in reducing the current uncertainty and the spread of data between different studies is to move to whole-rock studies rather than single-mineral studies. The understanding of the uncertainty related to CO_2 fluid properties would be greatly

enhanced by the availability of more comprehensive IFT and CA studies, at reservoir pressure and temperature conditions using core-flooding experiments and employing X-ray microtomography techniques (e.g. Andrew *et al.* 2014).

In summary, the IFT values for CO_2 are similar to those of oil, while methane IFT values are higher on average. The CAs in CO_2–brine system present a higher level of uncertainty and are hard to evaluate as a generic range. IFTs and CAs can, however, be defined with greater confidence for specific reservoir conditions, as exemplified by this study.

Conversion factor from hydrocarbons to CO_2

This work has defined an average value (μ) of the probability distributions of the IFT (39 mN m^{-1}) and CA (15°) for hydrocarbons under pressure and temperature conditions included in the calibration dataset by Yielding *et al.* (2010). This means that the calculated threshold capillary pressure of hydrocarbons can be converted to a CO_2–brine system for chosen IFT and CA values of CO_2:

$$P_c(CO_2) = P_c \frac{IFT_{CO_2} \cos\theta_{CO_2}}{\mu IFT_h \, \mu \cos\theta_h} \quad (6)$$

This can also be applicable to hydrocarbons in instances where the IFT and CA are well defined and significantly different to the average values.

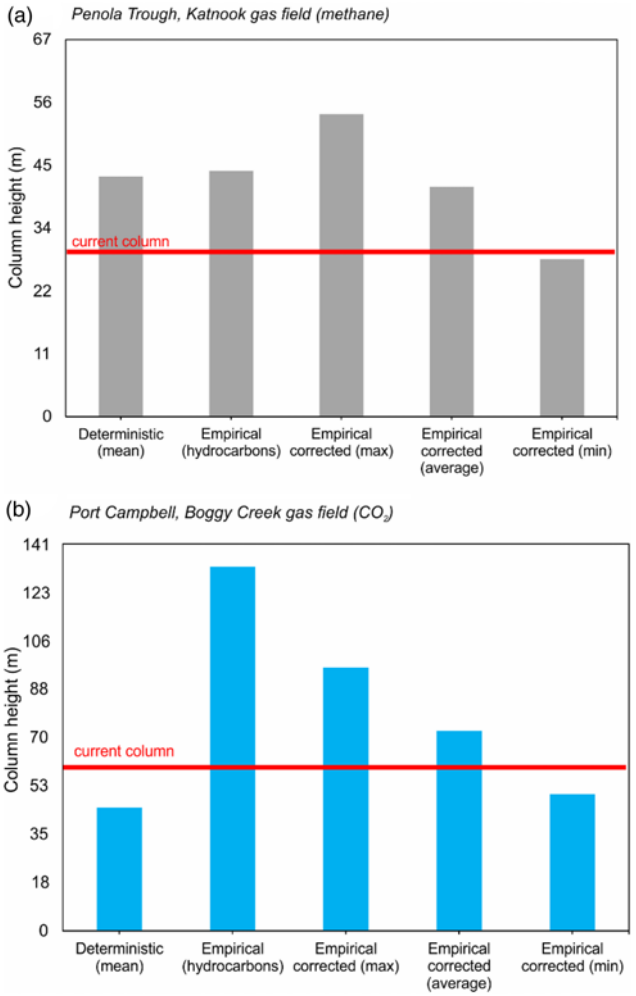

Fig. 13. Gas column heights: (**a**) Penola Trough, Katnook Field and (**b**) Port Campbell, Boggy Creek Field. Current live columns are marked in red. Models shown: deterministic (Sperrevik *et al.* 2002), empirical (Yielding *et al.* 2010), and empirical corrected maximum, average and minimum values (this work).

Figure 13 shows calculated column heights calculated using the standard empirical and deterministic methods, compared to the empirical model after conversion to CO_2 using equation (6) (maximum value) and calculated average and minimum values. For the Katnook methane system, the correction factor increases the column heights for methane due to a higher IFT but the overall change is not significantly different from the original empirical model. The current column is predicted to be stable regardless of the correction.

The maximum column height for the Boggy Creek CO_2 field is reduced by the correction, with the average empirical value slightly higher than the column height value known to be held by the fault. This prediction is in closer agreement to the deterministic model and is more likely to be correct based on the geochemistry of the fields, indicating higher mantle CO_2 contents at Boggy Creek than in the adjacent Buttress Field, and suggesting that initial charge to the Boggy Creek Field led to subsequent migration into the Buttress Field. The current column in Boggy Creek is not near the structural spill point, suggesting that the CO_2 transfer between the fields occurred through the fault rock, and the current column is therefore expected to be near the threshold value.

Conclusions

Two gas fields sealed by fault rocks were examined to compare the standard fault seal analysis techniques applied to methane–brine and CO_2–brine systems. In both cases, the column heights supported by the fault rocks were known, and geochemical gas analysis provided evidence for across-fault connectivity. This allowed us to assess and compare the strengths and weaknesses of two fault seal calibration methods (Sperrevik *et al.* 2002; Yielding *et al.* 2010).

The deterministic method predicted critical buoyancy pressure in the Katnook (methane) and Boggy Creek (CO_2) fields. The empirical method predicted critical buoyancy pressure in the Katnook Field and well below threshold pressure in the Boggy Creek Field. However, after accounting for uncertainty and applying the newly proposed correction for CO_2, the method also predicted criticality. Thus, the geochemistry and fault seal analysis results corroborate each other.

CO_2 fluid properties and their differences from hydrocarbons have been previously identified as the biggest uncertainty associated with fault seal application to CO_2 systems. However, an extensive literature review showed that a similar spread in interfacial tension (IFT) values exists within the hydrocarbons, due to the wide range of possible chemical compositions of crude oil. This means that the IFT in a CO_2–brine system is easier to identify for particular pressure and temperature conditions than in liquid hydrocarbons. Wettability of hydrocarbons is not very well characterized either, and the recent academic focus on CO_2 sequestration applications means that currently far more laboratory experimental data exist for CO_2–brine systems. Perhaps surprisingly, the main challenge in adapting fault seal modelling techniques from hydrocarbons to CO_2 is the uncertainty associated to the hydrocarbon properties.

The two fault seal prediction methods discussed here come with different inherent uncertainties and are best used in conjunction, bearing in mind the differences in the approach. The deterministic method (Sperrevik *et al.* 2002) can be applied to different fluids via the input of the IFT and contact angle (CA). This work has presented a similar conversion factor system to that applied to the empirical method (Bretan *et al.* 2003; Yielding *et al.* 2010). To do this, an average range of IFT and CA values in hydrocarbons under reservoir conditions were determined from the literature review. The percentage error related to the spread in fluid properties was calculated to be 24% of the calculated threshold capillary pressure value. This finding does not change the application of the empirical

method, which by definition provides a maximum estimate for capillary threshold pressures. However, it allows average and minimum capillary pressure values to be constrained, which can be used to ascertain 'most likely' and minimum column heights in hydrocarbon exploration. The newly defined average capillary threshold pressure value also allows for better comparison with the deterministic method, which by definition models average rather than maximum pressures.

In application to CO_2 storage, where a full column is fully or partially sealed by a fault, the buoyancy pressure must not exceed the minimum threshold capillary pressure value. However, the minimum values discussed here do not equate to safe or recommended buoyancy pressures for carbon capture and storage (CCS) contexts. Future studies should define the recommended limit in relation to the minimum threshold capillary pressure values defined here, based on risk analysis and regulatory guidelines.

The case study of the Boggy Creek CO_2 field demonstrates that IFTs can be very well constrained for particular target reservoir conditions. The definition of the CA remains more problematic because, in addition to the dependency on reservoir conditions and brine composition, the CA also depends on the chemical and textural properties of the fault/reservoir rock minerals. This presents two main issues: first, that the mineralogy and other properties such as the pore-space surface roughness of a particular target reservoir has to be known in detail – this should be easily overcome in the CCS context, where reservoir core studies will be undertaken before the final site selection; and, secondly, accurate measurements of the CA for the range of possible conditions. Recent whole-rock microtomography-based studies have started providing data from experimental set-ups that closely reflect real reservoir conditions (Andrew *et al.* 2014; Garing and Benson 2019). Future studies should expand these experiments to fault and phyllosilicate-rich rocks. As more data on fluid properties of hydrocarbons and CO_2 become available, the uncertainty related to conversion between the two systems will decrease.

Acknowledgements Badley Geoscience are thanked for the use of the TrapTester software and support throughout the project. We thank Peter Boult and Paul Lyon for providing 3D models of Penola Trough and Jennifer Ziesch for sharing the 3D model of Port Campbell and CO2CRC for providing the seismic data. Thanks to Eric Tenthorey for help with accessing the data and manuscript review.

Funding This work was supported by an EPSRC PhD studentship in partnership with CO2CRC and Badley Geoscience Ltd. Gareth Johnson was supported by EPSRC Grant EP/P026214/1 and the Faculty of Engineering at the University of Strathclyde.

Author contributions **RK**: conceptualization (lead), data curation (lead), formal analysis (lead), investigation (lead), methodology (lead), visualization (lead), writing – original draft (lead), writing – review & editing (lead); **GJ**: funding acquisition (lead), supervision (equal), writing – review & editing (supporting); **GY**: resources (lead), software (lead), supervision (equal), writing – review & editing (supporting); **SMVG**: funding acquisition (supporting), project administration (supporting), supervision (supporting).

References

Alipour Tabrizy, V., Denoyel, R. and Hamouda, A.A. 2011. Characterization of wettability alteration of calcite, quartz and kaolinite: Surface energy analysis. *Colloids and Surfaces A: Physicochemical and Engineering Aspects*, **384**, 98–108, https://doi.org/10.1016/j.colsurfa.2011.03.021

Allan, U.S. 1989. Model for hydrocarbon migration and entrapment within faulted structures. *AAPG Bulletin*, **73**, 803–811.

Andrew, M., Bijeljic, B. and Blunt, M.J. 2014. Pore-scale contact angle measurements at reservoir conditions using X-ray microtomography. *Advances in Water Resources*, **68**, 24–31, https://doi.org/10.1016/j.advwatres.2014.02.014

Arif, M., Al-yaseri, A.Z., Barifcani, A., Lebedev, M. and Iglauer, S. 2016. Impact of pressure and temperature on CO_2–brine–mica contact angles and CO_2–brine interfacial tension : Implications for carbon geo-sequestration. *Journal of Colloid and Interface Science*, **462**, 208–215, https://doi.org/10.1016/j.jcis.2015.09.076

Asquith, G.B., Krygowski, D. and Gibson, C.R. 2004. *Basic Well Log Analysis*. AAPG, Tulsa, OK.

Bachu, S. and Bennion, D.B. 2009. Interfacial tension between CO_2, freshwater, and brine in the range of pressure from (2 to 27) MPa, temperature from (20 to 125) °C, and water salinity from (0 to 334 000) mg L^{-1}. *Journal of Chemical & Engineering Data*, **54**, 765–775, https://doi.org/10.1021/je800529x

Barclay, S.A. and Worden, R.H. 2009. Effects of reservoir wettability on quartz cementation in oil fields. *International Association of Sedimentologists Special Publications*, **29**, 103–117, https://doi.org/10.1002/9781444304237.ch8

Bense, V.F., Shipton, Z.K., Kremer, Y. and Kampman, N. 2016. Fault zone hydrogeology: introduction to the special issue. *Geofluids*, **16**, 655–657, https://doi.org/10.1111/gfl.12205

Berg, R.R. 1975. Capillary pressures in stratigraphic traps. *AAPG Bulletin*, **59**, 939–956.

Bikkina, P.K. 2011. Contact angle measurements of CO_2–water–quartz/calcite systems in the perspective of carbon sequestration. *International Journal of Greenhouse Gas Control*, **5**, 1259–1271, https://doi.org/10.1016/j.ijggc.2011.07.001

Boreham, C.J., Hope, J.M. *et al.* 2004. Gas–oil–source correlations in the Otway Basin, southern Australia. *In*: Boult, P.J., Johns, D.R. and Lang, S.C. (eds) PESA's Eastern Australasian Basin Symposium II: Conference Proceedings. Petroleum Exploration Society of Australia (PESA), Perth, WA, Australia, 603–627.

Boult, P.J. and Hibburt, J.E. 2002. *The Petroleum Geology of South Australia. Volume 1: Otway Basin*. 2nd edn. Department of Primary Industries and Resources, Adelaide, SA, Australia.

Boult, P.J., Johns, D.R. and Lang, S.C. 2004. Subsurface plumbing of the Crayfish Group in the Penola Trough: Otway Basin. *In*: Boult, P.J., Johns, D.R. and Lang, S.C. (eds) *PESA's Eastern Australasian Basin Symposium II: Conference Proceedings*. Petroleum Exploration Society of Australia (PESA), Perth, WA, Australia, 483–498.

Boult, P., Lyon, P., Camac, B., Hunt, S. and Zwingmann, H. 2008. Unravelling the complex structural history of the Penola Trough – revealing the St George Fault. *In*: Blevin, J.E., Bradshaw, B.E. and Uruski, C. (eds) *PESA's Eastern Australasian Basin Symposium III: Conference Proceedings*. Petroleum Exploration Society of Australia (PESA), Perth, WA, Australia, 14–17.

Bouvier, J.D., Kaars-Sijpesteijn, C.H., Kluesner, D.F., Onyejekwe, C.C. and Van der Pal, R.C. 1989. Three-dimensional seismic interpretation and fault sealing investigations, Nun River Field, Nigeria. *AAPG Bulletin*, **73**, 1397–1414. https://doi.org/10.1306/44B4AA5A-170A-11D7-8645000102C1865D

Bretan, P. 2016. Trap Analysis: an automated approach for deriving column height predictions in fault-bounded traps. *Petroleum Geoscience*, **23**, 56–69, https://doi.org/10.1144/10.44petgeo2016-022

Bretan, P., Yielding, G. and Jones, H. 2003. Using calibrated shale gouge ratio to estimate hydrocarbon column heights. *AAPG Bulletin*, **87**, 397–413. https://doi.org/10.1306/08010201128

Bretan, P., Yielding, G., Mathiassen, O.M. and Thorsnes, T. 2011. Fault-seal analysis for CO_2 storage: an example from the Troll area, Norwegian Continental Shelf. *Petroleum Geoscience*, **17**, 181–192, https://doi.org/10.1144/1354-079310-025

Briguglio, D., Hall, M. and Keetley, J. 2015. Structural evolution of the Early Cretaceous depocentres, Otway Basin, Victoria. *Australian Journal of Earth Sciences*, 1–17, https://doi.org/10.1080/08120099.2015.1084048

Buckley, J.S., Liu, Y., Xie, X. and Morrow, N.R. 1997. Asphaltenes and crude oil wetting-the effect of oil composition. *SPE Journal*, **2**, 107–119, https://doi.org/10.2118/35366-PA

Chalbaud, C., Robin, M., Lombard, J.-M., Martin, F., Egermann, P. and Bertin, H. 2009. Interfacial tension measurements and wettability evaluation for geological CO_2 storage. *Advances in Water Resources*, **32**, 98–109, https://doi.org/10.1016/j.advwatres.2008.10.012

Chiquet, P., Daridon, J.-L., Broseta, D. and Thibeau, S. 2007*a*. CO_2/water interfacial tensions under pressure and temperature conditions of CO_2 geological storage. *Energy Conversion and Management*, **48**, 736–744, https://doi.org/10.1016/j.enconman.2006.09.011

Chiquet, P., Daridon, J.L., Broseta, D. and Thibeau, S. 2007*b*. CO_2/water interfacial tensions under pressure and temperature conditions of CO_2 geological storage. *Energy Conversion and Management*, **48**, 736–744, https://doi.org/10.1016/j.enconman.2006.09.011

Chivas, A.R., Barnes, I., Evans, W.C., Lupton, J.E. and Stone, J.O. 1987. Liquid carbon dioxide of magmatic origin and its role in volcanic eruptions. *Nature*, **326**, 587–589, https://doi.org/10.1038/326587a0

Cockshell, C.D., O'Brien, G.W., McGee, A., Lovibond, R., Perincek, D. and Higgins, R. 1995. Western Otway Crayfish Group troughs. *The APPEA Journal*, **35**, 385–404, https://doi.org/10.1071/AJ94025

Dance, T. 2013. Assessment and geological characterisation of the CO2CRC Otway Project CO_2 storage demonstration site: From prefeasibility to injection. *Marine and Petroleum Geology*, **46**, 251–269, https://doi.org/10.1016/j.marpetgeo.2013.06.008

Danesh, A. 1998. *PVT and Phase Behaviour of Petroleum Reservoir Fluids*. Elsevier, Amsterdam.

Daniel, R.F. and Kaldi, J.G. 2009. Evaluating seal capacity of cap rocks and intraformational barriers for CO2 containment. *AAPG Studies in Geology*, **59**, 335–345, https://doi.org/10.1306/13171247St59227

Duddy, I.R. 1997. Focussing exploration in the Otway Basin: understanding timing of source rock maturation. *The APPEA Journal*, **37**, 178–191, https://doi.org/10.1071/AJ96010

Espinoza, D.N. and Santamarina, J.C. 2010. Water–CO_2–mineral systems: Interfacial tension, contact angle, and diffusion – Implications to CO_2 geological storage. *Water Resources Research*, **46**, W07537, https://doi.org/10.1029/2009WR008634

Farokhpoor, R., Bjørkvik, B.J.A., Lindeberg, E. and Torsæter, O. 2013. CO_2 wettability behavior during CO_2 sequestration in saline aquifer – An experimental study on minerals representing sandstone and carbonate. *Energy Procedia*, **37**, 5339–5351, https://doi.org/10.1016/j.egypro.2013.06.452

Faulkner, D.R., Jackson, C.A.L., Lunn, R.J., Schlische, R.W., Shipton, Z.K., Wibberley, C.A.J. and Withjack, M.O. 2010. A review of recent developments concerning the structure, mechanics and fluid flow properties of fault zones. *Journal of Structural Geology*, **32**, 1557–1575, https://doi.org/10.1016/j.jsg.2010.06.009

Fisher, Q.J. and Knipe, R.J. 1998. Fault sealing processes in siliciclastic sediments. *Geological Society, London, Special Publications*, **147**, 117–134, https://doi.org/10.1144/GSL.SP.1998.147.01.08

Flock, D.L., Le, T.H. and Gibeau, J.P. 1986. The effect of temperature on the interfacial tension of heavy crude oils using the pendent drop apparatus. *Journal of Canadian Petroleum Technology*, **3**, 72–77, https://doi.org/10.2118/86-02-06

Fulljames, J.R., Zijerveld, L.J.J., Franssen, R., Møller-Pedersen, P. and Koestler, A.G. 1997. Fault seal processes: systematic analysis of fault seals over geological and production time scales. *Norwegian Petroleum Society Special Publications*, **7**, 51–59, https://doi.org/10.1016/S0928-8937(97)80006-9

Garing, C. and Benson, S.M. 2019. CO_2 wettability of sandstones: Addressing conflicting capillary behaviors. *Geophysical Research Letters*, **46**, 776–782, https://doi.org/10.1029/2018GL081359

Georgiadis, A., Maitland, G., Trusler, J.P.M. and Bismarck, A. 2010. Interfacial tension measurements of the ($H_2O + CO_2$) system at elevated pressures and temperatures. *Journal of Chemical & Engineering Data*, **55**, 4168–4175, https://doi.org/10.1021/je100198g

Ghorbani, M. and Mohammadi, A.H. 2017. Effects of temperature, pressure and fluid composition on hydrocarbon gas–oil interfacial tension (IFT): An experimental study using ADSA image analysis of pendant drop test method. *Journal of Molecular Liquids*, **227**, 318–323, https://doi.org/10.1016/j.molliq.2016.11.110

Gibson, R.G. 1998. Physical character and fluid-flow properties of sandstone-derived fault zones. Geological Society, London, Special Publications, **127**, 83–97, https://doi.org/10.1144/GSL.SP.1998.127.01.07

Gluyas, J.G. and Hichens, H.M. (eds). 2003. *United Kingdom Oil and Gas Fields: Commemorative Millennium Volume*. Geological Society, London, Memoirs, **20**, https://doi.org/10.1144/GSL.MEM.2003.020.01.01

Guariguata-Rojas, G.J. and Underhill, J.R. 2017. Implications of Early Cenozoic uplift and fault reactivation for carbon storage in the Moray Firth. *Interpretation*, **5**, SS1–SS21, https://doi.org/10.1190/int-2017-0009.1

Hassan, M.E., Nielsen, R.F. and Calhoun, J.C. 1953. Effect of pressure and temperature on oil–water interfacial tensions for a series of hydrocarbons. *Journal of Petroleum Technology*, **5**, 299–306, https://doi.org/10.2118/298-G

Higgs, K.E., Haese, R.R., Golding, S.D., Schacht, U. and Watson, M.N. 2015. The Pretty Hill Formation as a natural analogue for CO_2 storage: An investigation of mineralogical and isotopic changes associated with sandstones exposed to low, intermediate and high CO_2 concentrations over geological time. *Chemical Geology*, **399**, 36–64, https://doi.org/10.1016/j.chemgeo.2014.10.019

Hough, E.W., Rzasa, M.J. and Wood, B.B. 1951. Interfacial tensions at reservoir pressures and temperatures; apparatus and the water–methane system. *Journal of Petroleum Technology, AIME*, **2**, 57–60. https://doi.org/10.2118/951057-G

Iglauer, S. 2018. Optimum storage depths for structural CO_2 trapping. *International Journal of Greenhouse Gas Control*, **77**, 82–87, https://doi.org/10.1016/j.ijggc.2018.07.009

Iglauer, S., Pentland, C.H. and Busch, A. 2015. CO_2 wettability of seal and reservoir rocks and the implications for carbon geo-sequestration. *Water Resources Research*, **51**, 729–774, https://doi.org/10.1002/2014WR015553

Jung, J.-W. and Wan, J. 2012. Supercritical CO_2 and ionic strength effects on wettability of silica surfaces: equilibrium contact angle measurements. *Energy & Fuels*, **26**, 6053–6059, https://doi.org/10.1021/ef300913t

Kalantari Meybodi, M., Daryasafar, A. and Karimi, M. 2016. Determination of hydrocarbon–water interfacial tension using a new empirical correlation. *Fluid Phase Equilibria*, **415**, 42–50, https://doi.org/10.1016/j.fluid.2016.01.037

Karolytė, R. 2018. *The Migration and Retention of CO2 and Methane in the Otway Basin and South-east Australia: An Integrated Geochemical and Structural Analysis*. PhD thesis, University of Edinburgh, Edinburgh, UK.

Karolytė, R., Johnson, G., Györe, D., Serno, S., Flude, S., Stuart, F.M., Chivas, A.R., Boyce, A. and Gilfillan, S.M.V. 2019. Tracing the migration of mantle CO_2 in gas fields and mineral water springs in south-east Australia using noble gas and stable isotopes. *Geochimica et Cosmochimica Acta*, **259**, 109–128, https://doi.org/10.1016/j.gca.2019.06.002

Kashefi, K. 2012. *Measurement and Modelling of Interfacial Tension and Viscosity of Reservoir Fluids*. Doctoral thesis, Heriot-Watt University, Edinburgh, UK.

Knipe, R.J. 1997. Juxtaposition and seal diagrams to help analyze fault seals in hydrocarbon reservoirs. *AAPG Bulletin*, **81**, 187–195.

Lehner, F.K. and Pilaar, W.F. 1997. The emplacement of clay smears in synsedimentary normal faults: inferences from field observations near Frechen, Germany. *Norwegian Petroleum Society Special Publications*, **7**, 39–50, https://doi.org/10.1016/S0928-8937(97)80005-7

Lindsay, N.G., Murphy, F.C., Walsh, J.J., Watterson, J., Flint, S. and Bryant, I.D. 1993. Outcrop studies of shale smears on fault surfaces. *International Association of Sedimentologists Special Publications*, **15**, 113–123.

Lisk, M. 2004. Constraints on the oil prospectivity of the Penola Trough, onshore Otway Basin. *In*: Boult, P.J., Johns, D.R. and Lang, S.C. (eds) *PESA's Eastern Australasian Basin Symposium II: Conference Proceedings*. Petroleum Exploration Society of Australia (PESA), Perth, WA, Australia, 629–641.

Little, B.M. and Phillips, S.E. 1995. Detrital and authigenic mineralogy of the Pretty Hill Formation in the Penola Trough, Otway Basin: implications for future exploration and production. *The APPEA Journal*, **35**, 538–557, https://doi.org/10.1071/AJ94034

Liu, Y., Li, H.A. and Okuno, R. 2016. Measurements and modeling of interfacial tension for CO_2/CH_4/brine systems under reservoir conditions. *Industrial & Engineering Chemistry Research*, **55**, 12358–12375, https://doi.org/10.1021/acs.iecr.6b02446

Lovibond, R., Suttill, R.J., Skinner, J.E. and Aburas, A.N. 1995. The hydrocarbon potential of the Penola Trough, Otway Basin. *The APPEA Journal*, **35**, 358–371, https://doi.org/10.1071/AJ94023

Lyon, P.J., Boult, P.J., Mitchell, A. and Hillis, R.R. 2004. Improving fault geometry interpretation through 'pseudo-depth' conversion of seismic data in the Penola Trough, Otway Basin. *In*: Boult, P.J., Johns, D.R. and Lang, S.C. (eds) *PESA's Eastern Australasian Basin Symposium II: Conference Proceedings*. Petroleum Exploration Society of Australia (PESA), Perth, WA, Australia, 19–22.

Lyon, P.J., Boult, P.J., Hillis, R.R. and Mildren, S.D. 2005*a*. Sealing by shale gouge and subsequent seal breach by reactivation: A case study of the Zema Prospect, Otway Basin. *AAPG Hedberg Series*, **2**, 179–197, https://doi.org/10.1306/1060764H23169

Lyon, P.J., Boult, P.J., Watson, M.N. and Hillis, R. 2005*b*. A systematic fault seal evaluation of the Ladbroke Grove and Pyrus traps of the Penold Trough, Otway Basin. *The APPEA Journal*, **45**, 459–476, https://doi.org/10.1071/AJ04036

Lyon, P.J., Boult, P.J., Hillis, R.R. and Bierbrauer, K. 2007. Basement controls on fault development in the Penola Trough, Otway Basin, and implications for fault-bounded hydrocarbon traps. *Australian Journal of Earth Sciences*, **54**, 675–689, https://doi.org/10.1080/08120090701305228

Miocic, J.M., Gilfillan, S.M.V., Roberts, J.J., Edlmann, K., McDermott, C.I. and Haszeldine, R.S. 2016. Controls on CO_2 storage security in natural reservoirs and implications for CO_2 storage site selection. *International Journal of Greenhouse Gas Control*, **51**, 118–125, https://doi.org/10.1016/j.ijggc.2016.05.019

Miocic, J.M., Johnson, G. and Bond, C.E. 2019. Uncertainty in fault seal parameters: implications for CO_2 column height retention and storage capacity in geological CO_2 storage projects. *Solid Earth*, **10**, 951–967, https://doi.org/10.5194/se-10-951-2019

Najafi-Marghmaleki, A., Tatar, A., Barati-Harooni, A., Mohebbi, A., Kalantari-Meybodi, M. and Mohammadi, A.H. 2016. On the prediction of interfacial tension (IFT) for water–hydrocarbon gas system. *Journal of Molecular Liquids*, **224**, 976–990, https://doi.org/10.1016/j.molliq.2016.10.083

Naylor, M., Wilkinson, M. and Haszeldine, R.S. 2010. Calculation of CO_2 column heights in depleted gas fields from known pre-production gas column heights. *Marine and Petroleum Geology*, **28**, 1083–1093, https://doi.org/10.1016/j.marpetgeo.2010.10.005

Nordgard Bolas, H.M., Hermanrud, C. and Teige, G.M.G. 2005. Seal capacity estimation from subsurface pore pressures. *Basin Research*, **17**, 583–599, https://doi.org/10.1111/j.1365-2117.2005.00281.x

Øren, P.-E. and Bakke, S. 2003. Reconstruction of Berea sandstone and pore-scale modelling of wettability effects. *Journal of Petroleum Science and Engineering*, **39**, 177–199, https://doi.org/10.1016/S0920-4105(03)00062-7

Pei, Y., Paton, D.A., Knipe, R.J. and Wu, K. 2015. A review of fault sealing behaviour and its evaluation in siliciclastic rocks. *Earth-Science Reviews*, **150**, 121–138, https://doi.org/10.1016/j.earscirev.2015.07.011

Peng, D.-Y. and Robinson, D.B. 1976. A new two-constant equation of state. *Industrial & Engineering Chemistry Fundamentals*, **15**, 59–64, https://doi.org/10.1021/i160057a011

Radke, C.J., Kovscek, A.R. and Wong, H. 1992. A pore-level scenario for the development of mixed wettability in oil reservoirs. Paper SPE-24880 presented at the SPE Annual Technical Conference and Exhibition, 4–7 October 1992, Washington, DC, USA, https://doi.org/10.2118/24880-MS

Rajayi, M. and Kantzas, A. 2011. Effect of temperature and pressure on contact angle and interfacial tension of quartz/water/bitumen systems. *Journal of Canadian Petroleum Technology*, **50**, 61–67, https://doi.org/10.2118/148631-PA

Ren, Q.Y., Chen, G.J., Yan, W. and Guo, T.M. 2000. Interfacial tension of (CO_2 + CH_4) + water from 298K to 373K and pressures up to 30MPa. *Journal of Chemical & Engineering Data*, **45**, 610–612, https://doi.org/10.1021/je990301s

Rimstidt, J.D. and Barnes, H.L. 1980. The kinetics of silica–water reactions. *Geochimica et Cosmochimica Acta*, **44**, 1683–1699, https://doi.org/10.1016/0016-7037(80)90220-3

Schowalter, T.T. 1974. Mechanics of secondary hydrocarbon migration and entrapment, *AAPG Bulletin*, **63**, 723–760, https://doi.org/10.1306/2F9182CA-16CE-11D7-8645000102C1865D

Shipton, Z.K. and Cowie, P.A. 2001. Damage zone and slip-surface evolution over μm to km scales in high-porosity Navajo sandstone, Utah. *Journal of Structural Geology*, **23**, 1825–1844, https://doi.org/10.1016/S0191-8141(01)00035-9

Shipton, Z.K., Evans, J.P., Robeson, K.R., Forster, C.B. and Snelgrove, S. 2002. Structural heterogeneity and permeability in faulted eolian sandstone: Implications for subsurface modeling of faults. *AAPG Bulletin*, **86**, 863–883, https://doi.org/10.1306/61EEDBC0-173E-11D7-8645000102C1865D

Singh, K., Bijeljic, B. and Blunt, M.J. 2016. Imaging of oil layers, curvature and contact angle in a mixed-wet and a water-wet carbonate rock. *Water Resources Research*, **52**, 1716–1728, https://doi.org/10.1002/2015WR018072

Sneider, R.M., Sneider, J.S., Bolger, G.W. and Neasham, J.W. 1997. Comparison of seal capacity determinations: Conventional cores vs. cuttings. *AAPG Memoirs*, **67**, 1–12.

Sperrevik, S., Gillespie, P.A., Fisher, Q.J., Halvorsen, T. and Knipe, R.J. 2002. Empirical estimation of fault rock properties. *Norwegian Petroleum Society Special Publications*, **11**, 109–125. https://doi.org/10.1016/S0928-8937(02)80010-8

Sutjiadi-Sia, Y., Jaeger, P. and Eggers, R. 2008. Interfacial phenomena of aqueous systems in dense carbon dioxide. *The Journal of Supercritical Fluids*, **46**, 272–279, https://doi.org/10.1016/j.supflu.2008.06.001

Sutton, R.P. 2006. Oil system correlations. *In*: Fanchi, J.R. (ed.) *Petroleum Engineering Handbook, Volume 1: General Engineering*. Society of Petroleum Engineers, Richardson, TX, 258–306.

Tassone, D.R., Holford, S.P., Duddy, I.R., Green, P.F. and Hillis, R.R. 2014. Quantifying Cretaceous–Cenozoic exhumation in the Otway Basin, south-eastern Australia, using sonic transit time data: Implications for conventional and unconventional hydrocarbon prospectivity. *AAPG Bulletin*, **98**, 67–117, https://doi.org/10.1306/04011312111.

Teasdale, J.P., Pryer, L.L., Stuart-Smith, P.G., Romine, K.K., Etheridge, M.A., Loutit, T.S. and Kyan, D.M. 2003. Structural framework and basin evolution of Australia's southern margin. *The APPEA Journal*, **43**, 13–37, https://doi.org/10.1071/AJ02001

Tenthorey, E., Dance, T., Cinar, Y., Ennis-King, J. and Strand, J. 2014. Fault modelling and geomechanical integrity associated with the CO2CRC Otway 2C injection experiment. *International Journal of Greenhouse Gas Control*, **30**, 72–85, https://doi.org/10.1016/j.ijggc.2014.08.021

Tian, Y.-L., Xiao., Y.-F. *et al.* 1997. Interfacial tensions between water and non-polar fluids at high pressures and high temperatures. *Acta Physico-Chimica Sinica*, **13**, 89–95. https://doi.org/10.3866/PKU.WHXB19970120

Treiber, L.E. and Owens, W.W. 1972. A laboratory evaluation of the wettability of fifty oil-producing reservoirs. *Society of Petroleum Engineers Journal*, **12**, 531–540, https://doi.org/10.2118/3526-PA

Vavra, C.L., Kaldi, J.G. and Sneider, R.M. 1992. Geological applications of capillary pressure: a review (1). *AAPG Bulletin*, **76**, 840–850.

Watson, M.N., Zwingmann, N., Lemon, N.M. and Tingate, P.R. 2003. Onshore Otway Basin carbon dioxide accumulations: CO_2-induced diagenesis in natural analogues for underground storage of greenhouse gas. *The APPEA Journal*, **43**, 637–653, https://doi.org/10.1071/AJ02036

Watson, M.N., Boreham, C.J. and Tingate, P.R. 2004. Carbon dioxide and carbonate cements in the Otway Basin; implications for geological storage of carbon dioxide. *The APPEA Journal*, **44**, 703–720, https://doi.org/10.1071/AJ03035

Watts, N.L. 1987. Theoretical aspects of cap-rock and fault seals for single- and two-phase hydrocarbon columns. *Marine and Petroleum Geology*, **4**, 274–307, https://doi.org/10.1016/0264-8172(87)90008-0

Wiegand, G. and Franck, E.U. 1994. Interfacial tension between water and non-polar fluids up to 473 K and 2800 bar. *Berichte der Bunsengesellschaft für physikalische Chemie*, **98**, 809–817, https://doi.org/10.1002/bbpc.19940980608

Worden, R.H. and Morad, S. 2000. Economic evaluation of a petroleum accumulation demands a quartz cementation in oil field sandstones: a review of the key controversies. *International Association of Sedimentologists Special Publications*, **29**, 1–20, https://doi.org/10.1002/9781444304237.ch1

Yielding, G. 2002. Shale Gouge Ratio – calibration by geohistory. *Norwegian Petroleum Society Special Publications*, **11**, 1–15. https://doi.org/10.1016/S0928-8937(02)80003-0

Yielding, G. and Freeman, B. 2016. 3-D Seismic-Structural Workflows - Examples Using the Hat Creek Fault System, in: 3-D Structural Interpretation. *American Association of Petroleum Geologists*, 155–171, https://doi.org/10.1306/13561991M1111540

Yielding, G., Freeman, B. and Needham, D.T. 1997. Quantitative fault seal prediction. *AAPG Bulletin*, **81**, 897–917.

Yielding, G., Bretan, P. and Freeman, B. 2010. Fault seal calibration: a brief review. *Geological Society, London, Special Publications*, **347**, 243–255, https://doi.org/10.1144/SP347.14

Yielding, G., Lykakis, N. and Underhill, J.R. 2011. The role of stratigraphic juxtaposition for seal integrity in proven CO_2 fault-bound traps of the Southern North Sea. *Petroleum Geoscience*, **17**, 193–203, https://doi.org/10.1144/1354-0793/10-026

Ziesch, J., Aruffo, C.M. *et al.* 2015. Geological structure and kinematics of normal faults in the Otway Basin, Australia, based on quantitative analysis of 3-D seismic reflection data. *Basin Research*, **29**, 129–148, https://doi.org/10.1111/bre.12146

Ziesch, J., Aruffo, C.M. *et al.* 2017. Geological structure and kinematics of normal faults in the Otway Basin, Australia, based on quantitative analysis of 3-D seismic reflection data. *Basin Research*, **29**, 129–148, https://doi.org/10.1111/bre.12146